Langtaosha (LTS) Preprint doi: https://doi.org/10.65215/LTSpreprints.2026.10.20.000364. This version posted October 20, 2026. The copyright holder for this preprint (which was not certified by peer review) is the author/funder. Creative Commons license: CC Attribution-NonCommercial-NoDerivatives 4.0 https://creativecommons.org/licenses/by-nc-nd/4.0

Molecular Basis of Odorant Reception in the Asian Tiger Mosquito, *Aedes albopictus*

Qian Qi[1, 2#], Heng Zhang[1, 2#], Hui Yao[1], Fenglan Li[1], Dan Gou[1, 2], Simin Liang[1, 2], Rongrong Li[1, 2], Shan Li[1, 2], Mengli Chen[3*], Feng Liu[1, 2*]

1.Institute of Infectious Diseases, Shenzhen Bay Laboratory, Shenzhen, 518107, China

2.Guangdong Provincial Key Laboratory of Infection Immunity and Inflammation, Shenzhen, China

3.College of Advanced Agricultural Sciences, Zhejiang A&F University, Hangzhou, China

* Corresponding author

Feng Liu, Ph.D.
Infectious Diseases Research Institute, Shenzhen Bay Laboratory; Shenzhen, Guangdong 518132, China; Email: liufeng@szbl.ac.cn.

Mengli Chen, Ph.D.

College of Advanced Agricultural Sciences, Zhejiang A&F University, Hangzhou, 311300, China; Email: cmlmeng@zafu.edu.cn.

These authors contributed equally to this work.

Author Contributions

Conceived and designed the study: F.L., M.C. Performed the experiments: Q.Q., H.Z., H.Y., F.L., D.G., R L., S.L. Prepared the materials: Q.Q., D.G., S.L. Wrote and edited the paper: F.L., Q.Q., H.Z.

Competing Interest Statement: The authors declare no competing interests.

Classification: BIOLOGICAL SCIENCES, Neuroscience

Keywords: *Aedes albopictus*; olfaction; odorant receptors; single-flagellomere RNA-seq; terpenoids

This PDF file includes:

Main Text
Figures 1 to 6
Supplementary Figures 1 to 5
Supplementary Tables 1 to 3

Langtaosha (LTS) Preprint doi: https://doi.org/10.65215/LTSpreprints.2026.10.20.000364. This version posted October 20, 2026. The copyright holder for this preprint (which was not certified by peer review) is the author/funder. Creative Commons license: CC Attribution-NonCommercial-NoDerivatives 4.0 https://creativecommons.org/licenses/by-nc-nd/4.0

Abstract

As a major vector of multiple mosquito-borne diseases, the Asian tiger mosquito *Aedes albopictus* relies heavily on its olfactory system to detect attractive or aversive chemical cues during host seeking and habitat selection. However, the molecular mechanisms underlying odorant reception in *Ae. albopictus* remain largely elusive. In this study, we mapped the spatial distribution of odorant receptors (ORs) in the mosquito antenna using ultra-low input single-flagellomere RNA sequencing and the Q-binary reporter system. We identified a distinct spatial organization of ORs along the antenna: some ORs were uniformly expressed across flagellomeres (termed Uniform ORs), whereas others were preferentially enriched in the distal or proximal regions (termed Distal or Proximal ORs, respectively), thereby transcriptionally partitioning the antenna into distinct proximal and distal domains. We then successfully deorphanized 33 out of 68 annotated antennal tuning AalbORs, including 15 Distal, 10 Proximal, and 8 Uniform AalbORs, via the *Drosophila* “empty” neuron system, which exhibited robust responses to at least one compound from a comprehensive odorant panel spanning various chemical categories. Particularly, several narrowly tuned receptors were found to specialize in detecting ecologically relevant odorants, such as human-associated volatiles and plant-derived repellents. Moreover, *Ae. albopictus* ORs displayed significantly higher discriminability for ketones, alcohols, esters, aromatics, terpenoids, and heterocyclics compared with aldehydes and carboxylic acids, the latter of which were more likely recognized by ionotropic receptors. Notably, human-associated volatiles (e.g., alcohols, ketones, aromatics, and heterocyclics) were broadly recognized by ORs across all distribution patterns, whereas some terpenoids, previously reported as mosquito repellents, were preferentially detected by distally distributed ORs, suggesting potentially functional compartmentalization in the perception of aversive compounds. Collectively, this work provides novel insights into the chemosensory biology of *Ae. albopictus*, and may inform the development of innovative olfaction-based strategies for mosquito control.

Significance Statement

The Asian tiger mosquito, *Aedes albopictus,* is a globally invasive vector of arboviruses, yet the molecular basis of its odorant reception remains poorly understood. Here, via single-flagellomere transcriptomics sequencing and the Q-binary expression system, we present the first comprehensive spatial distribution map of odorant receptors (ORs) in this species, revealing a clear proximal–distal partition in terms of OR expression along the antenna. We also functionally deorphanize a majority of the female adult antennal ORs representing distinct spatial distribution patterns. We found that some human-associated volatiles are broadly recognized by ORs across all distribution patterns, whereas the plant-derived terpenoids—common constituents of essential oil repellents—are primarily detected by distally enriched ORs, suggesting a certain degree of functional compartmentalization of the antennal ORs in perceiving unfavorable odors. This study provides a foundational framework for understanding the basic olfactory physiology of mosquitoes, offering potential olfaction-based tactics for designing next-generation attractants or repellents to disrupt host-seeking behavior and interrupt disease transmission.

Langtaosha (LTS) Preprint doi: https://doi.org/10.65215/LTSpreprints.2026.10.20.000364. This version posted October 20, 2026. The copyright holder for this preprint (which was not certified by peer review) is the author/funder. Creative Commons license: CC Attribution-NonCommercial-NoDerivatives 4.0 https://creativecommons.org/licenses/by-nc-nd/4.0

Main Text

Introduction

The Asian tiger mosquito, *Aedes albopictus*, is a highly invasive insect species native to Southeast Asia that has expanded its geographic range to over 70 countries in recent decades. As a major mosquito vector, this species poses severe public health risks through the transmission of arboviruses, including dengue, Zika, and yellow fever viruses, via blood-feeding (1–3). This mosquito was also the primary vector of chikungunya virus, which led to the 2025 global epidemic with over 500,000 reported infection cases (4). Moreover, climate change has accelerated *Ae. albopictus* mosquitoes' expansion, and their growing resistance to conventional insecticides further complicates global control efforts (5).

Female *Ae. albopictus* mosquitoes feed on a broad range of vertebrate hosts for blood sources, which are essential for their egg development. In contrast to more anthropophilic mosquitoes, such as *Aedes aegypti* and *Anopheles gambiae*, *Ae. albopictus* displays opportunistic feeding behavior, which likely contributes to its population proliferation (6). In addition to seeking blood, this species actively forages across diverse natural habitats to locate favorable resting sites and floral sugar sources for energy. Therefore, it is crucial to understand how *Ae. albopictus* navigates chemically complex environments to identify an animal host for blood feeding and flowering plants for sugar feeding.

Mosquitoes rely heavily on their olfactory system, with the antennae, maxillary palps, and labella serving as the major olfactory appendages, to locate blood or sugar sources. Olfactory sensory neurons (OSNs) housed in the hair-like sensilla are critical for detecting semiochemicals derived from the hosts and natural environments. These volatile compounds are recognized by olfactory receptors, including odorant receptors (ORs) and ionotropic receptors (IRs), expressed on the membrane of OSNs (7, 8). Studies in *Drosophila melanogaster* and other insects have demonstrated that ORs form heteromeric ion channels with an obligate co-receptor ORCO and a ligand-sensitive tuning OR that mediates the detection of a broad range of chemical classes, such as ketones, alcohols, aromatics, and heterocyclics, whereas tuning IRs form ion channels with co-receptors (e.g., IR8a, IR76b, and IR25a) to detect heat (9), humidity (10), as well as chemicals, such as amines, acids, and/or certain aldehydes (11–13).

As the major olfactory appendage, the antenna of *Ae. albopictus* is slender and composed of the scape, pedicel, and the flagellum, which consists of 13 flagellomeres. All olfactory sensilla and OSNs are distributed along these flagellomeres. However, no study has been conducted on the distribution and/or functional pattern of ORs among different flagellomeres of the mosquito antenna. In *Drosophila*, distinct clusters of OSNs are distributed on the antenna with clear regional specificity (14). Similarly, in *An. gambiae*, certain antennal-expressed IRs are organized into proximal and distal domains (15). Such spatial distribution patterns suggest that olfactory receptors are probably not randomly expressed in the OSNs of different flagellomeres.

To date, within the family Culicidae, only the ORs of *An. gambiae* have been systematically characterized through both the *Drosophila "*empty" neuron system (16) and *Xenopus* oocytes

Langtaosha (LTS) Preprint doi: https://doi.org/10.65215/LTSpreprints.2026.10.20.000364. This version posted October 20, 2026. The copyright holder for this preprint (which was not certified by peer review) is the author/funder. Creative Commons license: CC Attribution-NonCommercial-NoDerivatives 4.0 https://creativecommons.org/licenses/by-nc-nd/4.0

expression system (17). The ORs of *Aedes* and *Culex* mosquitoes are sporadically deorphanized. For instance, OR4 and OR54 of *Ae. aegypti* were found to respond to the human-enriched sulcatone and the repellent DEET, respectively (18, 19); OR136 and OR32 of *Culex quinquefasciatus* were reported to recognize the repellent DEET and the oviposition cue p-cresol, respectively (20, 21). For *Ae. albopictus*, only four ORs have been functionally characterized against a narrow panel of compounds, including OR2, OR10, OR88, and OR11 (22–25). The functions of the majority of *Ae. albopictus* ORs remain largely elusive, leaving a considerable gap in our understanding of the molecular basis of odorant reception in this important disease vector.

Here, we comprehensively examined the spatial expression patterns of *Ae. albopictus* ORs along the flagellomeres of mosquito antennae by utilizing ultra-low-input single-flagellomere RNA-seq to create a detailed spatial distribution map. Our single-flagellomere transcriptomic data demonstrate a clear proximal-distal partition of the antenna in terms of OR expression, which was further validated by the Q-binary reporter system that localized specific ORs in the antenna through genetic fluorescence labeling. *Ae. albopictus* ORs can be readily classified into distally, proximally, and uniformly distributed groups. To further explore the potential linkage between the spatially distributed ORs and their functional specificity, we systematically deorphanized *Ae. albopictus* ORs using the *Drosophila* “empty” neuron system against a broad panel of odorants spanning various chemical categories, and unraveled the response spectra of 33 ORs exhibiting robust responses to at least one compound. Interestingly, we found that aromatics and heterocyclics, which share close chemical features, appear to be detected by the same set of ORs across all distribution patterns (distal, proximal, and uniform). Notably, the terpenoids, which are common constituents of mosquito-repelling essential oils, were preferentially detected by distally expressed ORs, suggesting a compartmentalized coding mode for perceiving terpenoids in the antenna of *Ae. albopictus*, which may correlate with the ecological significance of certain terpenoids in unfavorable habitats. By revealing the spatial expression and functional pattern of *Ae. albopictus* ORs, we provide novel insights into how distinct antennal OSNs are organized to decode complex chemical environments. This study not only deepens our understanding of the odor coding properties of the mosquito peripheral olfactory system but also contributes to the design of new attractants or repellents by interfering with odor detection in *Ae. albopictus*.

Results

Spatial distribution patterns of odorant receptors in the antennae of *Ae. albopictus*

The flagellum of the female *Ae. albopictus* antenna comprises 13 morphologically comparable flagellomeres, which house abundant OR-expressing OSNs (26). To characterize the spatial distribution of *OR*s in *Ae. albopictus* antennae, we conducted a single-flagellomere transcriptomic analysis using ultra-low-input RNA-seq following a modified Smart-seq2 protocol, a typical method used for full-length single-cell RNA-seq with enhanced transcript coverage, yield, and sensitivity, which enables detection of low-abundance genes and isoforms. Specifically, individual female antennal flagellomeres were freshly dissected and lysed; then full-length cDNA was synthesized with Sc reverse transcriptase and pre-amplified by limited-

Langtaosha (LTS) Preprint doi: https://doi.org/10.65215/LTSpreprints.2026.10.20.000364. This version posted October 20, 2026. The copyright holder for this preprint (which was not certified by peer review) is the author/funder. Creative Commons license: CC Attribution-NonCommercial-NoDerivatives 4.0 https://creativecommons.org/licenses/by-nc-nd/4.0

cycle PCR. Amplified cDNA was assessed for size distribution, and product sizes showing a major peak of 1000-2000 bp were selected for library construction. Sequencing libraries were subsequently generated and sequenced with a depth of approximately 60X. Clean reads were aligned to the *Ae. albopictus* transcript sequences of the NCBI RefSeq assembly AalbF5 and transcript abundance of genes was quantified after length normalization and bias correction (Fig. 1A).

A repertoire of 68 *AalbOR* genes was annotated based on this single-flagellomere transcriptomic dataset. Subsequent hierarchical clustering of flagellomeres based on the transcript abundance of *AalbORs* using Pearson correlation revealed a distinct spatial segregation of the flagellum into two domains: the proximal domain including flagellomeres 1-8, and the distal domain including flagellomeres 9-13 (Fig. 1B). Accordingly, *Ae. albopictus ORs* could be readily clustered into three groups: 29 distally enriched *AalbOR*s (Distal ORs, red-highlighted); 27 proximally enriched *AalbOR*s (Proximal ORs, blue-highlighted); 12 uniformly distributed *AalbOR*s and *ORCO* across the antennae (Uniform ORs, gray-highlighted) (Fig. 1C).

Validation of spatial expression patterns of *Ae. albopictus* ORs via the Q-binary reporter system

To verify the spatial expression patterns of *Ae. albopictus* ORs identified via single-flagellomere RNA-seq, we employed the Q-system to visualize *AalbORs* expression using fluorescent reporters. First, we examined the distribution of the OR co-receptor ORCO throughout the entire antenna. We leveraged a previously generated *AalbOrco-QF2* driver line by inserting an in-frame T2A-QF2-3xP3-DsRed cassette into the coding sequence of *AalbOrco* in addition to an effector line, QUAS-*mCD8*: GFP (26). Crossing the *AalbOrco-QF2* driver line with the QUAS-GFP effector line drives GFP expression in AalbOrco-positive OSNs in the antenna. Consistent with the single-flagellomere RNA-seq data, we observed a universal distribution of ORCO-positive GFP-labeled neurons across all 13 flagellomeres (Fig. 2A). Next, we focused on preferentially expressed tuning ORs by constructing driver lines using the promoters of specific *AalbORs*. We cloned *AalbORs*' promoter regions of different lengths (1.5k, 2k, and 5k bp) and integrated the pAalbOR-T2A-QF2-3XP3-DsRed cassette into the mosquito genome through piggybac-mediated random insertion. We initially screened eight proximal and ten distal AalbORs. Through exhaustive trials, we were able to establish five distal and three proximal OR driver lines. After crossing with the effector line, we only observed GFP-labeled OSNs in the antennae of progeny derived from two proximal OR driver lines (*AalbOR99* and *AalbOR43a*) and one distal driver line (*AalbOR41*). We examined and quantified 34, 36, and 21 antennae of *pAalbOR99-QF2>QUAS-mCD8:GFP*, *pAalbOR43a-QF2>QUAS-mCD8:GFP* and *pAalbOR41-QF2>QUAS-mCD8:GFP* mosquitoes, respectively. The distributions of GFP-labeled OSNs recapitulated the expression patterns of *AalbOR99* and *AalbOR43a* identified by the single-flagellomere RNA-seq, with a clear proximally biased expression (Fig. 2B, 2C). Furthermore, no GFP-labeled neurons were observed in flagellomeres 9–13 of the antenna for both lines (Fig. 2E, 2F). In contrast, *AalbOR41* expression was mainly concentrated (90%) in the distal region (flagellomeres 9–13), with 10% of neurons located in the 8th flagellomere (Fig. 2D, 2G). Collectively, the spatial localizations of these AalbOR-expressing OSNs unraveled by GFP-mediated genetic labeling confirmed the distribution patterns of *AalbORs* demonstrated by the

Langtaosha (LTS) Preprint doi: https://doi.org/10.65215/LTSpreprints.2026.10.20.000364. This version posted October 20, 2026. The copyright holder for this preprint (which was not certified by peer review) is the author/funder. Creative Commons license: CC Attribution-NonCommercial-NoDerivatives 4.0 https://creativecommons.org/licenses/by-nc-nd/4.0

single-flagellomere RNA-seq analysis.

Genetic factors affecting the antennal distribution of *Ae. albopictus* ORs

Genetic factors, such as phylogenetic relationships and chromosomal distributions, have been previously reported to determine the spatial organization of mouse ORs in the main olfactory epithelium (27). To explore whether a similar genetic basis underlying the spatial distribution of *AalbORs* in the antenna, we systematically examined the phylogenetic relationships and chromosomal organization of these genes. Phylogenetic analysis revealed a certain degree of correlation between sequence similarity and spatial expression patterns in AalbORs. Approximately 46% (31/68) of phylogenetically clustered ORs exhibited a similar region-specific expression pattern along the antenna. For instance, closely related paralogs AalbOR116, 121, and 122 were predominantly expressed in the proximal flagellomeres. Notably, the 13 distally expressed ORs, including AalbOR63, 64, 94a, 45, 31a, 70, 30a, 24, 83c, 20, 22c, 42, and 22, formed a compact phylogenetic clade (Fig. 3A). The close phylogenetic relationships among *AalbORs* with comparable distribution patterns may result from gene duplication and expansion during long-term evolution, representing a critical adaptive strategy for mosquitoes to enhance their olfactory sensitivity to certain biologically critical compounds.

Furthermore, chromosomal mapping revealed that 76% (29/38) of AalbOR genes with particular antennal spatial distributions formed compact clusters in distinct genomic loci (Fig. 3B). For example, AalbOR33a/46, AalbOR63a/92a, and AalbOR36/52, which were proximally distributed in the mosquito antenna, resided closely on the first, second, and third chromosomes, respectively. AalbOR31a/70/30a/42/94a/45/63/64 and AalbOR83c/22c/20, which were distally distributed in the mosquito antenna, were clustered on the second and third chromosomes, respectively. Such chromosomal clustering of AalbORs may facilitate coordinated transcriptional regulation via shared chromosomal regulatory elements (e.g., enhancers, chromatin structures).

Functional deorphanization of AalbORs against a broad panel of compounds

After exploring the spatial distribution patterns of AalbORs along the mosquito antenna, we next sought to characterize the response profiles of AalbORs with distinct distribution patterns using the recently optimized *Drosophila* “empty” neuron system (28). Of the 68 *AalbOR* genes identified in our single-flagellomere RNA-seq data, 55 were successfully amplified from female antennal cDNA libraries to establish the *Drosophila* UAS-AalbOR strains. We systematically characterized their response profiles against a comprehensive panel of 180 compounds, including both plant-derived and human-emitted volatiles, reflecting the mosquito’s reliance on plant sources for sugar acquisition and blood feeding for reproduction. Specifically, plant-derived volatiles in the test panel primarily included terpenoids (29) as typical plant secondary metabolites and esters from floral scents and fruit aromas (30). In contrast, human-emitted volatiles mainly consisted of skin secretions and microbial metabolites, including some ketones, aldehydes, alcohols, aromatics, heterocyclics, and carboxylic acids (31, 32). Notably, we intentionally included more plant-derived terpenoid and ester compounds than in previous studies on *Anopheles* mosquito ORs (16, 17) to minimize potential bias in the subsequent analysis.

In the control “empty” neuron driver strain (*OR22ab*$^{-/-}$*Gal4*), the endogenous A neuron

Langtaosha (LTS) Preprint doi: https://doi.org/10.65215/LTSpreprints.2026.10.20.000364. This version posted October 20, 2026. The copyright holder for this preprint (which was not certified by peer review) is the author/funder. Creative Commons license: CC Attribution-NonCommercial-NoDerivatives 4.0 https://creativecommons.org/licenses/by-nc-nd/4.0

(large amplitude spikes) of the ab3 sensillum exhibited minimal baseline activity and showed no response to ethyl acetate, whereas the B neuron (small amplitude spikes) responded robustly to 2-heptanone, collectively serving as reliable controls for sensillum identification. The ab3A neurons with heterologous expression of individual AalbOR displayed selective responses to specific chemical compounds; for instance, AalbOR6 was strongly activated by acetophenone, whereas AalbOR7a showed a potent response to linalool. This approach enabled us to comprehensively profile the responses of AalbORs to the large compound panel spanning 9 chemical categories. Ultimately, 33 AalbORs, including 15 Distal, 10 Proximal, and 8 Uniform AalbORs, were found to elicit excitatory responses (≥50 spikes/s) to at least one compound of the tested panel and to display distinct response spectra (Fig. 4B) that followed a dose-dependent manner (Fig. S1). Twenty AalbORs failed to be expressed in the *Drosophila* ab3A neuron, which showed no or burst large spikes in the extracellular recording and was insensitive to any compounds. Additionally, two AalbORs (AalbOR70 and AalbOR88) appeared to be normally expressed but showed no response to any compounds in our panel, possibly because their ligands are out of the odor panel in this study. Of note, some AalbORs presented preferential sensitivity to compounds of different chirality. For instance, AalbOR24 showed a significantly stronger response to (−)-α-pinene and S-(−)-limonene than to (+)-α-pinene and R-(+)-limonene (Fig. S2), suggesting their remarkable capability to distinguish different enantiomers of the same compounds in the peripheral olfactory system.

We generated tuning curves for responsive AalbORs (Fig. S3). As expected, some AalbORs had broad response spectra with relatively low kurtosis values (e.g., AalbOR39, 71a, and 24), whereas others were narrowly tuned with high kurtosis values (e.g., AalbOR2, 6, and 60). Notably, among the top eight ORs with the highest kurtosis values, half were specialized for detecting human-derived volatiles, such as AalbOR2 for indole, AalbOR6 for acetophenone, AalbOR60 for 2-decanol, and AalbOR63a for 3-methyl-1-butanol. The other half was dedicated to plant-derived volatiles, including AalbOR4 for eugenol, AalbOR104 for β-caryophyllene, AalbOR56a for fenchone, and AalbOR7a for linalool. This apparently balanced olfactory representation underscored the ecological importance of both host and plant cues in environmental navigation by *Ae. albopictus*.

Representation of odor space by AalbORs

After deorphanizing the response profiles of AalbORs, we next asked how odor space is represented by this receptor repertoire. We employed 32 molecular descriptors to represent the structural features of the odorants, consistent with the previous study in *An. gambiae* (16, 33). These descriptors encompass features such as the carbon chain length, functional groups, and number of aromatic hydroxyls. To visualize this 32-dimensional space, we applied principal components analysis (PCA) to project it into two dimensions and observed that compounds within the same chemical category tended to cluster together, whereas compounds from different categories were relatively well separated in this odor space (Fig. 5A). We then mapped the response intensities of 33 deorphanized AalbORs to each compound as bubble sizes (Fig. 5A), revealing that the response spectra of AalbOR repertoire covered a broad region of the odor space, with pronounced sensitivity to specific alcohols, terpenoids, ketones, aromatics, and esters.

Langtaosha (LTS) Preprint doi: https://doi.org/10.65215/LTSpreprints.2026.10.20.000364. This version posted October 20, 2026. The copyright holder for this preprint (which was not certified by peer review) is the author/funder. Creative Commons license: CC Attribution-NonCommercial-NoDerivatives 4.0 https://creativecommons.org/licenses/by-nc-nd/4.0

We also exploratorily integrated each AalbOR's expression level with its odor-evoked responses, which enables us to conceptually measure the olfactory receptivity of *AalbOR* repertoire to those compounds. Specifically, olfactory receptivity was calculated by multiplying the compound-evoked response value of each AalbOR by its transcription level (34). We found that *Ae. albopictus* exhibited the strongest receptivity to (+)-fenchone, 4-methylcyclohexanol, (−)-fenchone, and camphor (Fig. S4A). When closely examining the relative contributions of major AalbORs in perceiving these top four compounds, we found that AalbOR56a consistently played the predominant role (Fig. S4B). Interestingly, AalbOR56a was highly conserved between *Ae. albopictus* and *Ae. aegypti*. The ortholog AaegOR11 shares 92% amino acid identity with AalbOR56a and also shows strong sensitivity to both (+)- and (−)-fenchone (35), suggesting a potentially conserved responsiveness to (+) or (−)-fenchone in both *Aedes* mosquitoes. Indeed, Yan et al. (24) demonstrated that (+)-fenchone exhibited strong repellency against *Ae. albopictus* and this repellency was significantly reduced when AalbOR56a (also named AalbOR11 in Yan et al. (24)) was knocked down by RNA interference.

We subsequently evaluated the discriminating ability of *Ae. albopictus* ORs toward major chemical classes by calculating the mean Euclidean distances within each chemical category (36). Our analysis revealed that the largest mean Euclidean distances were observed within ketones and alcohols, suggesting that AalbORs could effectively differentiate structural variations within these compound groups. Of note, the mean Euclidean distances among aldehydes and carboxylic acids were significantly smaller than those of other compound groups, suggesting that they may be less likely to be discriminated by *Ae. albopictus* ORs, in line with previous findings regarding the low sensitivity of insect ORs to aldehydes and acids (17, 23) (Fig. 5B). In addition to ketones and alcohols, several other chemical classes, including esters, aromatics, terpenoids, and heterocyclics, presented intermediate Euclidean distances larger than those of aldehydes and acids, suggesting they can be more robustly discriminated by *Ae. albopictus* ORs (Fig. 5C). These findings indicated distinct capabilities of *Ae. albopictus* ORs in distinguishing different compounds in their environment.

Correlation between the spatial distribution and functional specificity of AalbORs.

To investigate the potential sensory preference of differentially distributed AalbORs for various odorants, we specifically examined the compounds that evoked at least one extremely strong response (≥150 spikes/s) across the functionally characterized AalbORs repertoire. Interestingly, while some odorants (e.g., ethyl hexanoate, cyclohexanone, and 4-methylcyclohexanol) were recognized by multiple AalbORs with distinct spatial distributions, others were selectively detected by a few AalbORs with specific distribution patterns (Fig. 6A, Fig. S5). For instance, several alcohols, including 1-octanol, trans-2-octen-1-ol, and 2-decanol, were consistently recognized by the same panel of AalbORs mainly with proximal distribution in the antenna, including AalbOR76, 79, 39, and 43a. In contrast, some plant-derived terpenoids, such as (-)-fenchone, (+)-fenchone, and camphor, were primarily recognized by mostly distally distributed AalbORs, including AalbOR50, 63, 104, 7a, 30a, 24, and 71a. Moreover, some odorants were narrowly encoded by one or two AalbORs with distinct spatial distributions. For example, indole was specifically recognized by proximally distributed AalbOR2, whereas plant-

Langtaosha (LTS) Preprint doi: https://doi.org/10.65215/LTSpreprints.2026.10.20.000364. This version posted October 20, 2026. The copyright holder for this preprint (which was not certified by peer review) is the author/funder. Creative Commons license: CC Attribution-NonCommercial-NoDerivatives 4.0 https://creativecommons.org/licenses/by-nc-nd/4.0

derived linalool, (-)-linalool, and linalyl acetate were mainly recognized by the distally distributed AalbOR7a. Similarly, human-associated acetophenone, 1-indanone, and 2-acetylthiathene, were perceived by distally distributed AalbOR6 and AalbOR24. This result indicated that the mosquito antenna adopted a compartmentalized strategy to encode certain compounds of potential ecological relevance.

Additionally, we investigated the recognition pattern of AalbORs to odors of different chemical classes. The response preference of AalbORs for major chemical categories was evaluated by the Response Index (RI), which was calculated by dividing the ratio of one AalbOR's active excitatory response (≥50 spikes/s) induced by compounds of the same category by the proportion of that chemical category in the test panel. This index indicates the response specificity or preference of individual AalbORs against particular chemical categories. As expected, we found that most groups of compounds, including human-associated volatiles (including alcohols, ketones, aromatics, and heterocyclics) and plant-derived esters, were detected by multiple AalbORs across all types of spatial distribution. Among them, alcohols, ketones, and esters were the most broadly recognized by multiple AalbORs, whereas aromatics and heterocyclics were relatively narrowly responded by a few AalbORs (Fig. 6B). Of note, a similar subset of AalbORs detected aromatics and heterocyclics, likely attributing to their shared chemical structures, such as the benzene ring in these compounds (Fig. 6B). Intriguingly, we found one group of mainly distally distributed AalbORs (seven distally and one uniformly, but no proximally distributed AalbORs) that were highly specialized in detecting terpenoids, suggesting the spatial aggregation of certain AalbORs with remarkable functional consensus in sensing terpenoids in *Ae. albopictus* (Fig. 6B).

Discussion

The *Ae. albopictus* mosquito relies on its sophisticated olfactory system to navigate complex chemical environments rich in both 'favorable' host cues and 'adverse' signals, including human odorants and chemical repellents. As a major type of chemosensory receptor, odorant receptors of *Ae. albopictus* play an indispensable role in detecting volatiles encountered during host seeking and environmental exploration. This study comprehensively characterized, for the first time, the spatial distribution and functional response profiles of odorant receptors in *Ae. albopictus*. We uncovered the distinctive compartmentalization of AalbORs in both expression patterns and functional properties, revealing the spatially and functionally advanced organization of AalbORs within the mosquito antenna. This correlation between spatial distribution and functional specificity provides a foundational framework for understanding the chemosensory physiology of mosquitoes and offers potential targets for disrupting their olfaction-mediated behavior through targeted interventions.

This study revealed that while some *AalbORs* are uniformly expressed across the flagellomeres of the antenna, a subset of AalbORs are preferentially clustered in the proximal region, and others are enriched in the distal part. This distribution pattern is potentially shaped by their genetic phylogeny and chromosomal organization. Similarly, previous work on the distribution of IRs in *Anopheles coluzzii* showed that some AcolIRs are expressed in the "proximal" section,

Langtaosha (LTS) Preprint doi: https://doi.org/10.65215/LTSpreprints.2026.10.20.000364. This version posted October 20, 2026. The copyright holder for this preprint (which was not certified by peer review) is the author/funder. Creative Commons license: CC Attribution-NonCommercial-NoDerivatives 4.0 https://creativecommons.org/licenses/by-nc-nd/4.0

while others are restricted to the “distal” part (15), suggesting that both mosquito IRs and ORs may adopt a similar distribution pattern along the antenna. Furthermore, the spatial partitioning of AalbORs into proximal and distal sectors mirrors a certain degree of functional compartmentalization, which may facilitate the integration of information from chemical signals in the natural environment. Indeed, our functional characterization of AalbORs indicated that terpenoids tend to be recognized by distal AalbORs. This spatial and functional compartmentalization of ORs has also been extensively reported in the model insect *D. melanogaster* (14, 37, 38), suggesting that it may be a general rule across different insect species.

Functional studies indicated that *Anopheles gambiae* ORs (*AgamORs*) are more sensitive to aromatics than to esters, whereas *Drosophila* ORs (*DmelORs*) tend to respond to esters rather than aromatics (16, 17). This was proposed to be associated with the haematophagous requirements of *Anopheles* mosquitoes and the fruit-seeking activity of flies. However, in this study, we revealed that AalbORs exhibited robust responses and discriminating ability toward esters in addition to aromatics. This discrepancy may be attributed to two factors: species-specific differences and/or variations in the compound panels. Specifically, our screening panel encompassed a better-balanced set of esters and aromatics (26 esters and 26 aromatics), in contrast to the 11 esters versus 18 aromatics used by Carey et al. (16), which would increase the probability of biased detection toward aromatics. Moreover, beyond blood feeding, mosquitoes, similar to flies, also depend heavily on plant fluid or floral nectar for basic carbohydrate nutrition. Indeed, many fragrances released by fruits and flowers are attractive to mosquitoes (39–41). For example, Leon-Noreña et al. (42) reported that mango (*Mangifera indica*), peach (*Prunus persica*), and banana (*Musa acuminata*) are enriched with ester volatiles (e.g., isoamyl acetate), which elicit strong electroantennography (EAG) responses in the mosquito antennae and exert strong behavioral attraction toward *Ae. aegypti*. Therefore, it is also ecologically meaningful for mosquitoes to detect esters as important cues for energy sources.

In addition, terpenoids, another major category of plant secondary metabolites, have been neglected in previous studies on the response spectra of *AgamORs* and *DmelORs*, yet were particularly examined in this work. We found that terpenoids represent an important group of compounds that serve as extremely sensitive ligands for distally expressed AalbORs within the mosquito antenna, highlighting the ecological significance of terpenoids in *Ae. albopictus*. Indeed, several studies have shown that terpenoids are major components of mosquito-repelling essential oils. For instance, linalool, which was specifically recognized by AalbOR7a, is a major component of camphor oil (43); β-caryophyllene, the strongest activator of AalbOR104, was identified as the major constituent of *Carpesium abrotanoides* oil (44); and the widely used EPA-approved natural mosquito repellent Lemon Eucalyptus Oil is mainly composed of terpenoids, including eucalyptol, limonene, citronellol, citral, and myrcene (45), which elicited strong responses in several distally distributed AalbORs, such as AalbOR71a and AalbOR24. Interestingly, the synthetic mosquito repellent DEET has also been reported to activate the OR54 located in the distal section (Flagellomeres 10-13) of the antenna in *Ae. aegypti* (19), suggesting that both *Ae. aegypti* and *Ae. albopictus* may adopt a similar paradigm

Langtaosha (LTS) Preprint doi: https://doi.org/10.65215/LTSpreprints.2026.10.20.000364. This version posted October 20, 2026. The copyright holder for this preprint (which was not certified by peer review) is the author/funder. Creative Commons license: CC Attribution-NonCommercial-NoDerivatives 4.0 https://creativecommons.org/licenses/by-nc-nd/4.0

to perceive aversive compounds via the distal antennae during foraging.

Moreover, AalbORs exhibited the strongest responses and prominent distinguishing ability toward ketones, as well as some aromatics and heterocyclics. Analyses of human body odors indicate that ketones, aromatics, and heterocyclics are major constituents of the volatile profile emitted by human skin (46–48). Specifically, the ketone sulcatone, which generated the largest response in AalbOR83c and AalbOR22c, was previously reported as the key compound that distinguishes humans from animals in *Ae. aegypti* (18). Additionally, the aromatic acetophenone, the most robust agonist for AalbOR6, was found to be the crucial chemical cue responsible for the enhanced attraction of dengue-infected human hosts to *Aedes* mosquitoes (49). Interestingly, the heterocyclic indole, which triggered the most potent response in AalbOR2, was found to significantly inhibit mosquito attraction toward human hands and long-range host-seeking behavior (50), suggesting its potential role as an endogenous repellent released from the human body. All three categories of compounds were broadly detected by distally, proximally, and uniformly expressed AalbORs, suggesting their fundamental roles in host-seeking and blood-feeding behaviors.

Materials and Methods

Mosquito maintenance. The *Ae. albopictus* Foshan strain was kindly provided by Dr. Xiaoguang Chen (Southern Medical University). For all experiments, non-blood-fed female mosquitoes aged 4 to 7 days old were used. All mosquito colonies were maintained in an insectary at the Shenzhen Bay Laboratory under controlled conditions: 27 °C, 75% relative humidity, a 12 h light:12 h dark photoperiod, and were supplied with a 10% sucrose solution.

Single-flagellomere RNA-seq.

Sample Collection and Lysis. *Ae. albopictus* female adults at 5 days post-eclosion were cold-anesthetized on ice. Individual antennal flagellomeres were dissected and immediately placed into low-binding PCR tubes containing lysis buffer and RNase inhibitor (Vazyme, N712). Samples were flash-frozen in liquid nitrogen to ensure complete cellular disruption.

cDNA synthesis and amplification. Full-length cDNA was synthesized using the Vazyme N712 kit following a SMART-seq2 protocol. Oligo(dT)VN primers captured poly(A)+ mRNA, and Sc Reverse Transcriptase-mediated template switching appended a universal 5’ sequence to the first-strand cDNA via TSO (template-switching oligos) annealing. Full-length double-stranded cDNA was then pre-amplified by limited-cycle PCR using universal primers.

Library construction and quality control. Amplified cDNA was purified with AMPure XP beads at a bead-to-sample ratio of 0.8:1, quantified using a Qubit, and assessed for size distribution using an Agilent Bioanalyzer to confirm the expected product size of around 1000-2000 bp. Sequencing libraries were prepared using the Vazyme TruePrep Flexible DNA Library Prep Kit (Vazyme, TD504).

Sequencing and data analysis. Libraries were sequenced on an Illumina NovaSeq X Plus platform with 150-bp paired-end reads. Raw sequencing reads were quality-filtered and adapter-trimmed using Trim Galore! (version 0.6.10), with a minimum Phred quality score of 25 and a minimum read length of 36 bp. Clean reads were quantified against the *Ae. albopictus* transcript sequences of NCBI RefSeq assembly AalbF5 (GCF_035046485.1) using Salmon

Langtaosha (LTS) Preprint doi: https://doi.org/10.65215/LTSpreprints.2026.10.20.000364. This version posted October 20, 2026. The copyright holder for this preprint (which was not certified by peer review) is the author/funder. Creative Commons license: CC Attribution-NonCommercial-NoDerivatives 4.0 https://creativecommons.org/licenses/by-nc-nd/4.0

(version 2.7.0) with mapping validation enabled.

PiggyBac-mediated microinjection and laser confocal microscopy imaging. To generate the *pAalbOr-QF2* driver line, the piggyBac transposon system was used to generate transgenic strains for inserts of interest. Inserts were cloned into pBac vector by Gibson Assembly and verified by Sanger sequencing. pBac vector pBac-OpIE2-DsRed was linearized by XhoI and used as the backbone. A genomic fragment containing the upstream promoter regions (5 kb, 2 kb, or 1.5 kb) and 5' UTR of ten distal AalbORs (OR94a, OR64, OR20, OR41, OR13a, OR50, OR6, OR83c, OR67c, OR71a) and eight proximal AalbORs (OR99, OR84, OR79, OR76, OR117, OR39, OR43a, OR92a) was amplified from *Ae. albopictus* genomic DNA using PCR. Primers used for generating the *AalbORs-QF2* driver lines are listed in Table S1. The mixtures of transgene plasmids (300 ng/μL) and piggyBac transposase expression plasmid pUC19-OpIE2-DsRed-pAaUb-transposase (200 ng/μL) were injected into ~300 *Ae. albopictus* embryos. G0 females were outcrossed to wild-type *Ae. albopictus* males. Positive individuals in G1 were then outcrossed to wild-type *Ae. albopictus* for 3 more generations to establish the stable transgenic strains. Offspring individuals were screened based on their DsRed-derived red-eye fluorescence and subsequently crossed with a QUAS-GFP effector line generated via piggyBac transposition (QUAS-mCD8:GFP-3xP3-ECFP) (26). Crossing these lines drives GFP expression in AalbOr-expressing cells. Transgenic larvae were identified by eye-specific DsRed and ECFP fluorescence. Then the antennae were dissected with an insect pin and directly imaged the GFP-labeled sensory neurons using a confocal laser scanning microscope.

RNA extraction and UAS-Or construct generation. To generate UAS-Or constructs, we employed the homologous recombination method. The antennae of one hundred mosquitoes were dissected on ice and immediately transferred into Trizol reagent (Invitrogen, Carlsbad, CA, USA) for RNA extraction. cDNA was synthesized from 1 μg of total RNA using the HiScript® III 1st Strand cDNA Synthesis Kit (Vazyme Biotech Co., Ltd, Nanjing, China) according to the manufacturer's instructions. To amplify the full-length coding sequence of AalbOr, primers with homology arms were designed based on the coding sequence of the putative AalbOr available in VectorBase (https://www.vectorbase.org) (Supplementary Table 2). The PUAS-attB vector was used as a template and amplified using Phusion® High-Fidelity DNA Polymerase (New England Biolabs, Ipswich, MA, USA) to generate the linearized vector using primers PUAS-attB-F (5'-GAATTCGTTAACAGATCTGCG-3') and PUAS-attB-R (5'-GAATTCCCAATTCCCTATTCA-3'). The AalbOR fragment was then ligated into the linearized vector using the pEASY-Basic Seamless Cloning and Assembly Kit (TransGen Biotech, Beijing, China), and the resulting construct was transformed into Trans1-T1 Phage Resistant Chemically Competent Cells (TransGen Biotech, Beijing, China). The recombinant plasmid was purified using the Plasmid Mini Kit II (Omega Bio-Tek, Norcross, GA, USA) and subsequently microinjected into *Drosophila* embryos.

AalbOR-expression in *Drosophila* empty neuron system. We followed the protocol described by John Carlson (Yale University) for the heterologous expression of AalbORs in the ab3A empty neurons. The fly crossing protocol consisted of two steps: replacing the wild-type phenotype with balancer markers and introducing the mosquito *OR* gene into the ab3A empty

Langtaosha (LTS) Preprint doi: https://doi.org/10.65215/LTSpreprints.2026.10.20.000364. This version posted October 20, 2026. The copyright holder for this preprint (which was not certified by peer review) is the author/funder. Creative Commons license: CC Attribution-NonCommercial-NoDerivatives 4.0 https://creativecommons.org/licenses/by-nc-nd/4.0

neuron. The UAS-Or constructs were microinjected into fly strains harboring a rescue gene for the white-eye phenotype, producing transgenic flies with red eyes and a genotype of *w; +; UAS-Or(w+)/+*. The ab3A mutant line (*Or22ab$^{-/-}$Gal4/CyO*) and the balancer line (*Sp/CyO; Dr/TM3*) were generously provided by John Carlson (Yale University). From these two lines, we first generated the intermediate fly line *Or22ab$^{-/-}$Gal4/CyO; Dr/TM3*, which exhibits curly wings and stubble bristles. Then we self-crossed this line to obtain the homozygous empty neuron line *Or22ab$^{-/-}$Gal4; Dr/TM3*, with straight wings and stubble bristles. In parallel, the U*AS-Or* line, which carries the mosquito *Or* gene under UAS control, was used to generate the balanced *UAS-Or* line (*Sp/CyO; UAS-Or/TM3*), displaying curly wings and stubble bristles. This balanced line was then crossed with *Or22ab$^{-/-}$Gal4; Dr/Tm3* to produce *Or22ab$^{-/-}$Gal4/CyO*; *UAS-Or/TM3*, which exhibits orange eyes, curly wings, and stubble bristles. Finally, this line was self-crossed to establish the stable and homozygous fly line for single sensillum recording: *Or22ab$^{-/-}$ Gal4/Or22ab$^{-/-}$Gal4; UAS-Or/UAS-Or,* which displays red eyes and straight wings.

Single sensillum recordings. Single sensillum recordings (SSR) were conducted as described in Liu et al (51). Flies of homozygous line *Or22ab$^{-/-}$Gal4/Or22ab$^{-/-}$Gal4; UAS-Or/UAS-Or* aged 4–10 days post-eclosion, were used for recordings. A female fly was wedged into the narrow end of a truncated plastic pipette tip and placed on a slide. The tip of a glass micropipette was used to hold the antenna in a stable position. Once mounted, the specimen was placed under a microscope (Eclipse FN1, Japan) and the antenna was viewed at high magnification (1000×). Two tungsten microelectrodes were sharpened in 10% KNO_2 solution at 10 V. The reference electrode, which was connected to ground, was inserted into the compound eye of the *Drosophila*, and the other was connected to the preamplifier (10×, Syntech, Kirchzarten, Germany) and inserted into the shaft of an olfactory sensillum to complete the electrical circuit for extracellular recording of ab3 sensillum potentials. 2-heptanone, which exclusively stimulates B neurons in the ab3 sensillum, was used to differentiate the correct ab3 sensillum. Controlled manipulation of the electrodes was performed using a micromanipulator (Burleigh PCS-6000, CA). The preamplifier was connected to an analog-to-digital signal converter (IDAC-4, Syntech, Germany), which in turn was connected to a computer for signal recording and visualization in the software AutoSpike v5.1. Signals were recorded for 10 s starting 1 s before stimulation, and the action potentials were counted offline automatically with the AutoSpike software over a 500-ms period before and after stimulation. The spontaneous firing rates observed in the preceding 500 ms were subtracted from the total spike rates observed during the 500-ms stimulation, and counts were calculated in units of spikes/s. Compounds that were used in single sensillum recordings are listed in Supplementary Table S3.

Bioinformatic and evolutionary analyses were conducted as described below. Hierarchical clustering of the flagellomeres based on *AalbORs* transcript abundance, functional clustering based on SSR results, and chromosomal distribution of ORs were analyzed using TBtools-II (Toolbox for Biologists) v2.472. Phylogenetic trees of AalbOR amino acid sequences were constructed using MEGA12 via the maximum likelihood (ML) method. For chemometric analysis, principal component analysis (PCA) was applied to generate two-dimensional projections of the AalbOR-defined odor space using GraphPad Prism 10, and to visualize intra-class odorant dispersion in three dimensions using Origin 2026.

Langtaosha (LTS) Preprint doi: https://doi.org/10.65215/LTSpreprints.2026.10.20.000364. This version posted October 20, 2026. The copyright holder for this preprint (which was not certified by peer review) is the author/funder. Creative Commons license: CC Attribution-NonCommercial-NoDerivatives 4.0 https://creativecommons.org/licenses/by-nc-nd/4.0

Acknowledgements

We thank all members of the Feng Liu Lab at Shenzhen Bay Laboratory and the Mengli Chen Lab at Zhejiang A&F University for suggestions and comments. We thank Yanjie Wang at the Genomics Core, Biomedical Research Core Facilities, Shenzhen Bay Laboratory, for technical support and assistance with the development of a Smart-seq2-based protocol for micro-tissue samples. We also thank the Mosquito Gene Editing Service Center (Biosafety Level 2, BSL-2), for providing mosquito embryo injection services and the (Animal Biosafety Level 2, ABSL-2) Laboratories of the Institute of Infectious Diseases, Shenzhen Bay Laboratory, for their support and assistance during this research.

Reference

1. S. Leta, et al. Global risk mapping for major diseases transmitted by *Aedes aegypti* and *Aedes albopictus*. *Int. J. Infect. Dis.* 67, 25-35 (2018).
2. G. Benelli, R. Petrelli, A. Canale. Arthropod-borne disease control at a glance: what's new on drug development? *Molecules* 25, 5175 (2020).
3. V. Battaglia, et al. The worldwide spread of *Aedes albopictus*: new insights from mitogenomes. *Front. Genet.* 13, 931163 (2022).
4. World Health Organization. Chikungunya-Global situation. (2025).
5. J. Vontas, et al. Insecticide resistance in the major dengue vectors *Aedes albopictus* and *Aedes aegypti*. *Pestic. Biochem. Physiol.* 104, 126-131 (2012).
6. W. A. Hawley. The biology of *Aedes albopictus*. *Journal of the American Mosquito Control Association* 4, 2-39 (1988).
7. A. F. Carey, J. R. Carlson. Insect olfaction from model systems to disease control. *Proc. Natl. Acad. Sci. USA* 108, 12987-12995 (2011).
8. W. S. Leal. Odorant reception in insects: roles of receptors, binding proteins, and degrading enzymes. *Annu. Rev. Entomol.* 58, 373-391 (2013).
9. C. Greppi, W. J. Laursen, G. Budelli, E. C. Chang, A. M. Daniels, L. Van Giesen, A. L. Smidler, F. Catteruccia, P. A. Garrity. Mosquito heat seeking is driven by an ancestral cooling receptor. *Science* 367, 681-684 (2020).
10. W. J. Laursen, G. Budelli, R. Tang, E. C. Chang, R. Busby, S. Shankar, R. Gerber, C. Greppi, R. Albuquerque, P. A. Garrity. Humidity sensors that alert mosquitoes to nearby hosts and egg-laying sites. *Neuron* 111, 874-887 (2023).
11. R. M. Joseph, J. R. Carlson. Drosophila chemosensors: diverse neurons, complex molecular detectors. *Curr. Biol.* 25, R199-R207 (2015).
12. A. F. Silbering, R. Rytz, Y. Grosjean, L. Abuin, P. Ramdya, G. S. X. E. Jefferis, R. Benton. Complementary function and integrated wiring of the evolutionarily distinct *Drosophila* olfactory subsystems. *J. Neurosci.* 31, 13357-13375 (2011).
13. R. Benton, K. S. Vannice, C. Gomez-Diaz, L. B. Vossall. Variant ionotropic glutamate receptors as chemosensory receptors in *Drosophila*. *Cell* 136, 149-162 (2009).

Langtaosha (LTS) Preprint doi: https://doi.org/10.65215/LTSpreprints.2026.10.20.000364. This version posted October 20, 2026. The copyright holder for this preprint (which was not certified by peer review) is the author/funder. Creative Commons license: CC Attribution-NonCommercial-NoDerivatives 4.0 https://creativecommons.org/licenses/by-nc-nd/4.0

14. M. de Bruyne, K. Foster, J. R. Carlson. Odor coding in the *Drosophila* antenna. *Neuron* 30, 537-552 (2001).
15. J. I. Raji, J. K. Konopka, C. J. Potter. A spatial map of antennal-expressed ionotropic receptors in the malaria mosquito. *Cell Rep.* 42, 112101 (2023).
16. A. F. Carey, G. Wang, C. Y. Su, L. J. Zwiebel, J. R. Carlson. Odorant reception in the malaria mosquito *Anopheles gambiae*. *Nature* 464, 66-71 (2010).
17. R. Haddad, et al. A metric for odorant comparison. Nat. Methods 5, 425-429 (2008).
18. G. Wang, A. F. Carey, J. R. Carlson, L. J. Zwiebel. Molecular basis of odor coding in the malaria vector mosquito *Anopheles gambiae*. *Proc. Natl. Acad. Sci. USA* 107, 4418-4423 (2010).
19. C. S. McBride, et al. Evolution of mosquito preference for humans linked to an odorant receptor. *Nature* 515, 222-227 (2014).
20. X. Wang, et al. DEET olfactory reception in the yellow fever mosquito. LangTaoSha Preprint Server (2026).
21. P. Xu, Y. M. Choo, A. De La Rosa, W. S. Leal. Mosquito odorant receptor for DEET and methyl jasmonate. *Proc. Natl. Acad. Sci. USA* 111, 16592-16597 (2014).
22. P. Xu, et al. Odorant inhibition in mosquito olfaction. *iScience* 19, 524-532 (2019).
23. F. Scialò, B. S. Hansson, E. Giordano, C. L. Polito, F. A. Digilio. Molecular and functional characterization of the odorant receptor2 (OR2) in the tiger mosquito *Aedes albopictus. PLoS One* 7, e36538 (2012).
24. H. Liu, et al. Functional analysis of Orco and odorant receptors in odor recognition in *Aedes albopictus*. *Parasit. Vectors* 9, 363 (2016).
25. R. Yan, et al. A potential link between aromatics-induced oviposition repellency behaviors and specific odorant receptor of *Aedes albopictus*. *Pest Manag Sci.* 80, 3603-3611 (2024).
26. R. Yan, et al. Molecular and functional characterization of a conserved odorant receptor from *Aedes albopictus*. *Parasit. Vectors* 15, 43 (2022).
27. H. Yao, et al. Unveiling the developmental dynamics and functional role of odorant receptor co-receptor (Orco) in *Aedes albopictus*: a novel mechanism for regulating odorant receptor expression. *PLoS Negl. Trop. Dis.* 19, e0013753 (2025).
28. B. Bintu, Y. Isogai, I. Jenie, X. Zhuang, C. Dulac. Spatial organization and detection of social odors in mouse primary olfactory system. *Cell* 189, 3380-3397 (2026).
29. J. S. Chahda, et al. The molecular and cellular basis of olfactory response to tsetse fly attractants. *PLoS Genet.* 15, e1008005 (2019).
30. D. A. T. Boncan, S. S. Tsang, C. Li, I. H. Lee, H. M. Lam, T. F. Chan, J. H. Hui. Terpenes and terpenoids in plants: Interactions with environment and insects. *Int. J. Mol. Sci*. 21, 7382 (2020).
31. S. Mostafa, Y. Wang, W. Zeng, B. Jin. Floral scents and fruit aromas: Functions, compositions, biosynthesis, and regulation. *Front. Plant Sci*. 13, 860157 (2022).

Langtaosha (LTS) Preprint doi: https://doi.org/10.65215/LTSpreprints.2026.10.20.000364. This version posted October 20, 2026. The copyright holder for this preprint (which was not certified by peer review) is the author/funder. Creative Commons license: CC Attribution-NonCommercial-NoDerivatives 4.0 https://creativecommons.org/licenses/by-nc-nd/4.0

626 32. N. O. Verhulst, et al. Human skin microbiota and their volatiles as odour baits for the
627 malaria mosquito *Anopheles gambiae* s.s. *Entomol. Exp. Appl* 139, 170-179 (2011).
628 33. U. R. Bernier, et al. Analysis of human skin emanations by gas chromatography/mass
629 spectrometry. 2. Identification of volatile compounds that are candidate attractants for the
630 yellow fever mosquito (*Aedes aegypti*). *Anal. Chem*. 72, 747-756 (2000).
631 34. D. C. Rinker, R. J. Pitts, X. Zhou, E. Suh, A. Rokas, L. J. Zwiebel. Blood meal-induced
632 changes to antennal transcriptome profiles reveal shifts in odor sensitivities in *Anopheles*
633 *gambiae*. *Proc. Natl. Acad. Sci.* USA 110, 8260-8265 (2013).
634 35. W. Lu, W. S. Leal, K. K. Brisco, S. An, A. J. Cornel. A highly expressed odorant receptor
635 from the yellow fever mosquito, AaegOR11, responds to (+)- and (-)-fenchone and a
636 phenolic repellent. *Insect Biochem. Mol. Biol.* 151, 103866 (2022).
637 36. H. H. Sun, F. Liu, A. Baker, L. J. Zwiebel. Neuronal odor coding in the larval sensory cone
638 of *Anopheles coluzzii*. Complex responses from a simple system. *Cell Reports* 36, 109555
639 (2021).
640 37. A. Couto, M. Alenius, B. J. Dickson. Molecular, anatomical, and functional organization of
641 the *Drosophila* olfactory system. *Curr. Biol.* 15, 1535-1547 (2005).
642 38. P. Clyne, C. Warr, M. Freeman. A novel family of divergent seven-transmembrane proteins.
643 *Neuron* 22, 327-338 (1999).
644 39. D. M. Shannon, N. Richardson, C. Lahondere, D. Peach. Mosquito floral visitation and
645 pollination. *Curr. Opin. Insect Sci.* 65, 101230 (2024).
646 40. E. Barredo, M. DeGennaro. Not just from blood: mosquito nutrient acquisition from nectar
647 sources. *Trends Parasitol.* 36, 473-484 (2020).
648 41. G. C. Muller, R. D. Xue, Y. Schlein. Differential attraction of *Aedes albopictus* in the field
649 to flowers, fruits and honeydew. *Acta Trop.* 118, 45-49 (2011).
650 42. M. Leon-Norena, G. M. Tauxe, J. A. Riffell. Olfactory preferences and chemical differences
651 of fruit odors for *Aedes aegypti* mosquitoes. *J. Exp. Biol.* 228, 18 (2025).
652 43. E. Guenther. *The Essential Oils*, Vol. 4. Van Nostrand, New York (1950).
653 44. A. Haris, M. Azeem, M. Binyameen. Mosquito repellent potential of *Carpesium*
654 *abrotanoides* essential oil and its main components against a dengue vector, *Aedes*
655 *aegypti*. *J. Med. Entomol.* 59, 801-809 (2022).
656 45. F. Manzoor, N. Naz, S. A. Malik, S. Arshad, B. Siddiqui. Chemical composition of essential
657 oils derived from *Eucalyptus* and lemongrass and their antitermitic activities against
658 *Microtermes mycophagus*. *Asian J. Chem.* 24, 2405-2408 (2012).
659 46. J. Zhao, A. Q. Chen, J. Ryu, J. del Marmol. Structural basis of odor sensing by insect
660 heteromeric odorant receptors. *Science* 384, 1460-1467 (2024).
661 47. P. Mochalski, J. King, K. Unterkofler, H. Hinterhuber, A. Amann. Emission rates of selected
662 volatile organic compounds from skin of healthy volunteers. *J. Chromatogr. B* 959, 62-70
663 (2014).

Langtaosha (LTS) Preprint doi: https://doi.org/10.65215/LTSpreprints.2026.10.20.000364. This version posted October 20, 2026. The copyright holder for this preprint (which was not certified by peer review) is the author/funder. Creative Commons license: CC Attribution-NonCommercial-NoDerivatives 4.0 https://creativecommons.org/licenses/by-nc-nd/4.0

48. Z. Zou, X. Yang. Skin volatile organic compound emissions from 14 healthy young adults under controlled conditions. *Build Environ* 222, 109416 (2022).

49. H. Zhang, et al. A volatile from the skin microbiota of flavivirus-infected hosts promotes mosquito attractiveness. *Cell* 185, 2510-2522.e16 (2022).

50. A. Dekel, et al. The oviposition cue indole inhibits animal host attraction in *Aedes aegypti* mosquitoes. *Parasit. Vectors* 15, 422 (2022).

51. F. Liu, Z. Chen, N. Liu. Molecular basis of olfactory chemoreception in the common bed bug, *Cimex lectularius*. *Sci. Rep.* 7, 45531 (2017).

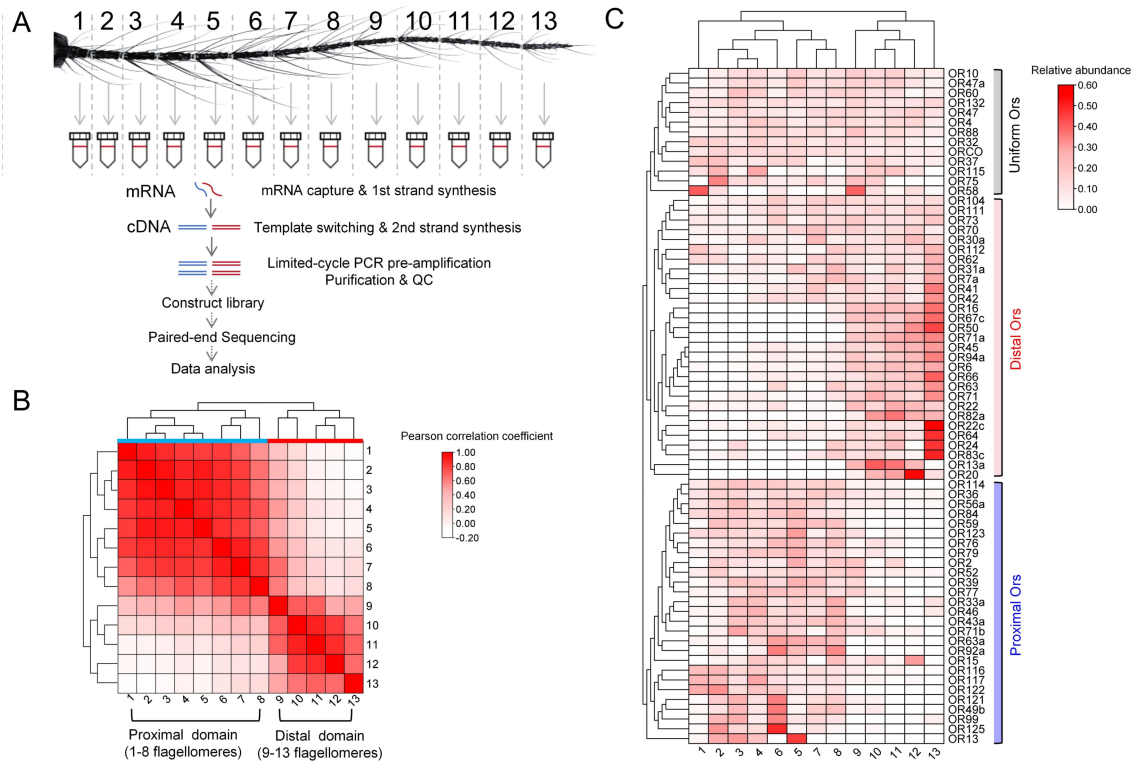


Figure 1. Spatial distribution patterns of *Ae. albopictus ORs* (*AalbORs*) in the antennae. (A) Schematic diagram of ultra-low-input RNA-seq for individual antennal flagellomeres of *Ae. albopictus*. (B) Hierarchical clustering of flagellomeres based on the transcript abundance of *AalbORs*. (C) Classification of *AalbORs* into three distribution categories according to spatial expression profiles across the flagellum. Red markers denote *AalbORs* with distal distribution, blue markers represent proximally enriched *AalbORs*, and gray markers indicate *AalbORs* with uniform expression across the entire antennal flagellum.

Langtaosha (LTS) Preprint doi: https://doi.org/10.65215/LTSpreprints.2026.10.20.000364. This version posted October 20, 2026. The copyright holder for this preprint (which was not certified by peer review) is the author/funder. Creative Commons license: CC Attribution-NonCommercial-NoDerivatives 4.0 https://creativecommons.org/licenses/by-nc-nd/4.0

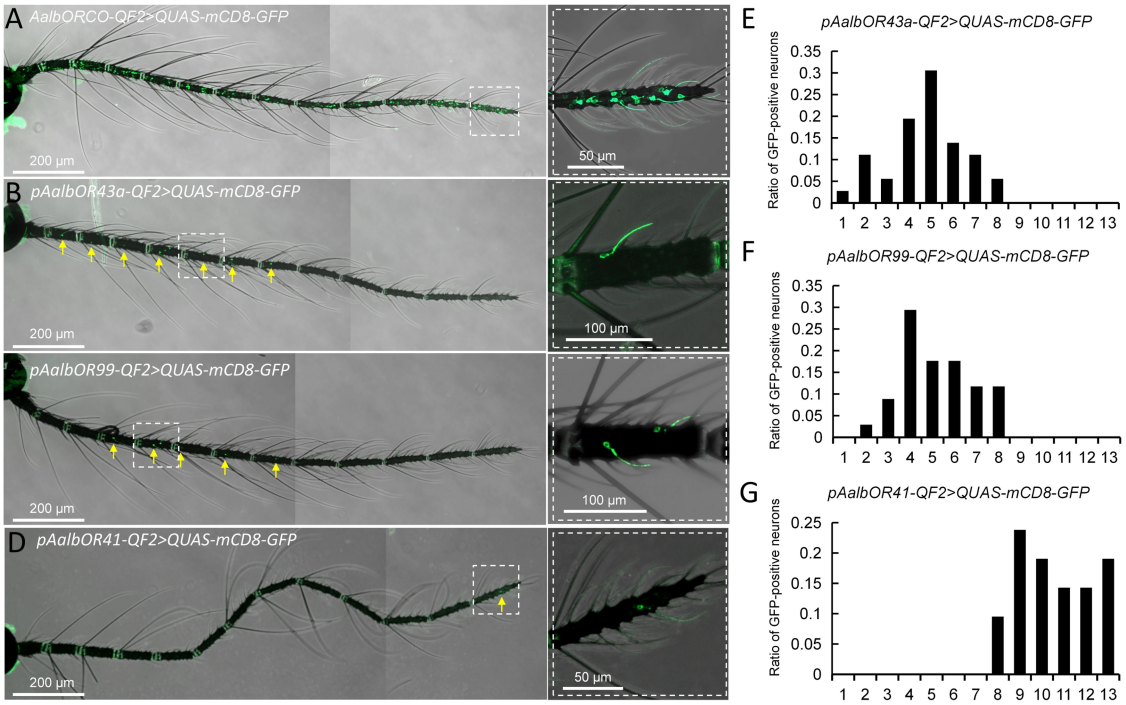
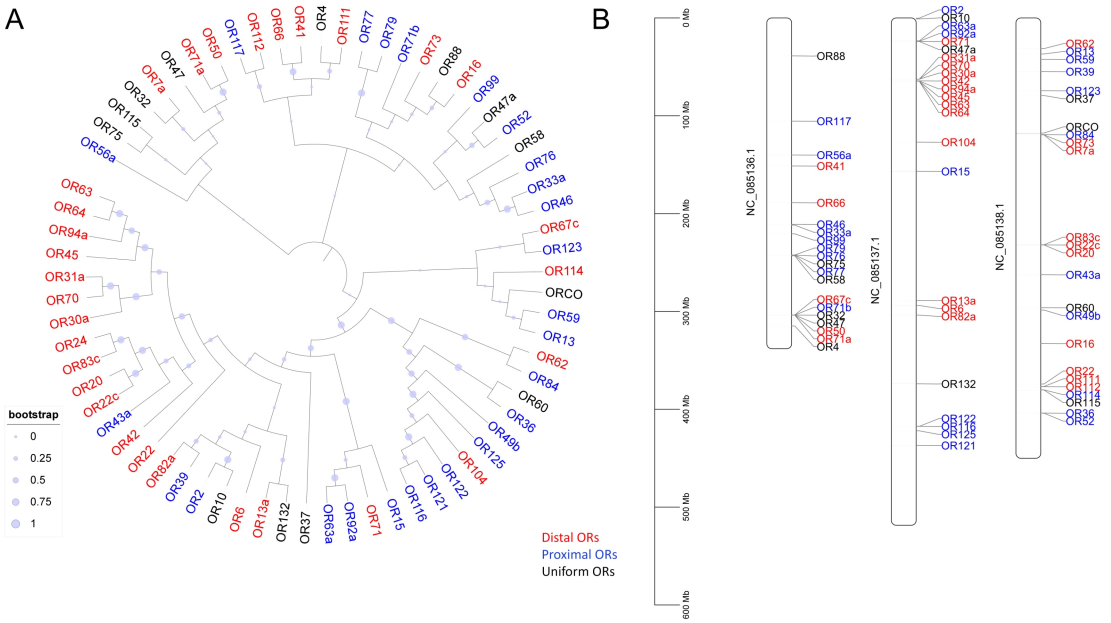


Figure 2. Validation of distal and proximal *Ae. albopictus* ORs through Q-binary reporter system. (A) Overview and magnified confocal images of GFP-labeled OSNs in a specific antennal flagellum of *AalbORCO-QF2>QUAS-mCD8-GFP* mosquitoes. Uniform GFP signals were detected in both proximal and distal regions of the antenna. (B) Confocal imaging showed the distribution of GFP-labeled OSNs in the proximal flagellomeres of the *AalbOR43a-QF2>QUAS-mCD8:GFP* mosquito. (C) Confocal imaging showed the distribution of GFP-labeled OSNs in the proximal flagellomeres of the *AalbOR99-QF2>QUAS-mCD8:GFP* mosquito. (D) Confocal imaging showed the distribution of GFP-labeled OSNs in the distal flagellomeres of the *AalbOR41-QF2>QUAS-mCD8:GFP* mosquito. White arrows denote the flagellomeres showing GFP-labeled OSNs. (E), (F), and (G) Ratio of GFP-labeled OSNs in individual flagellomeres of *pAalbOR43a-QF2>QUAS-mCD8-GFP*, *pAalbOR99-QF2>QUAS-mCD8-GFP*, and *pAalbOR41-QF2>QUAS-mCD8-GFP*, respectively.

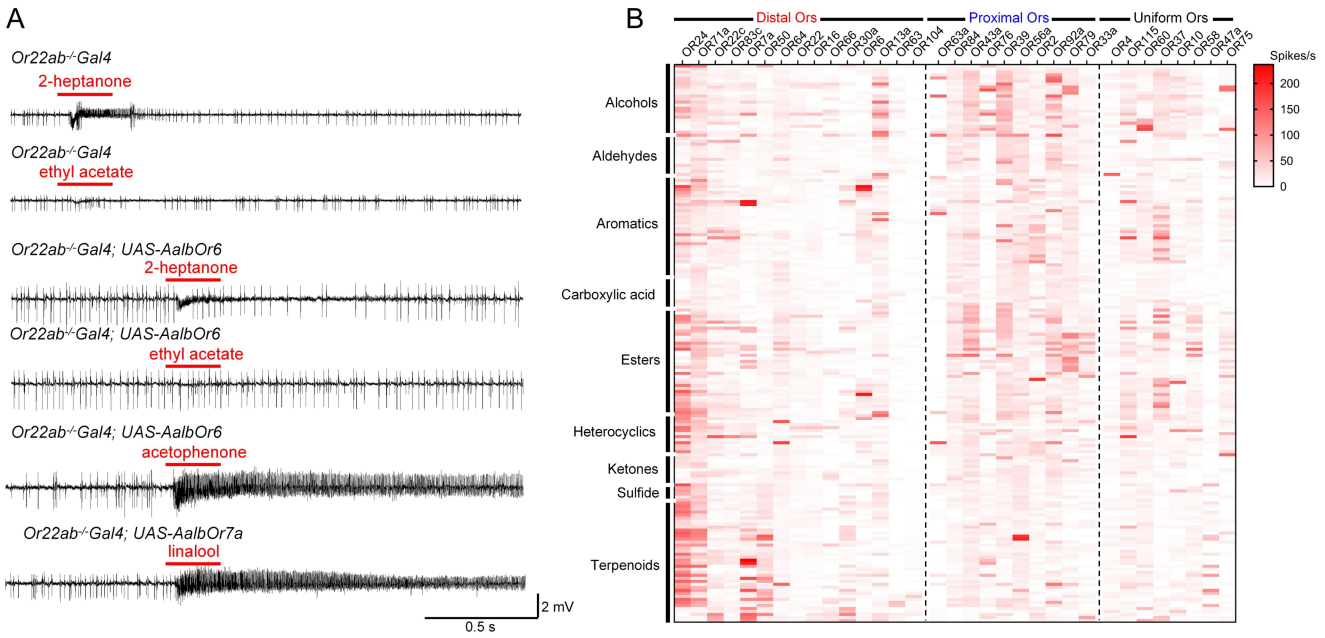
Langtaosha (LTS) Preprint doi: https://doi.org/10.65215/LTSpreprints.2026.10.20.000364. This version posted October 20, 2026. The copyright holder for this preprint (which was not certified by peer review) is the author/funder. Creative Commons license: CC Attribution-NonCommercial-NoDerivatives 4.0 https://creativecommons.org/licenses/by-nc-nd/4.0



694

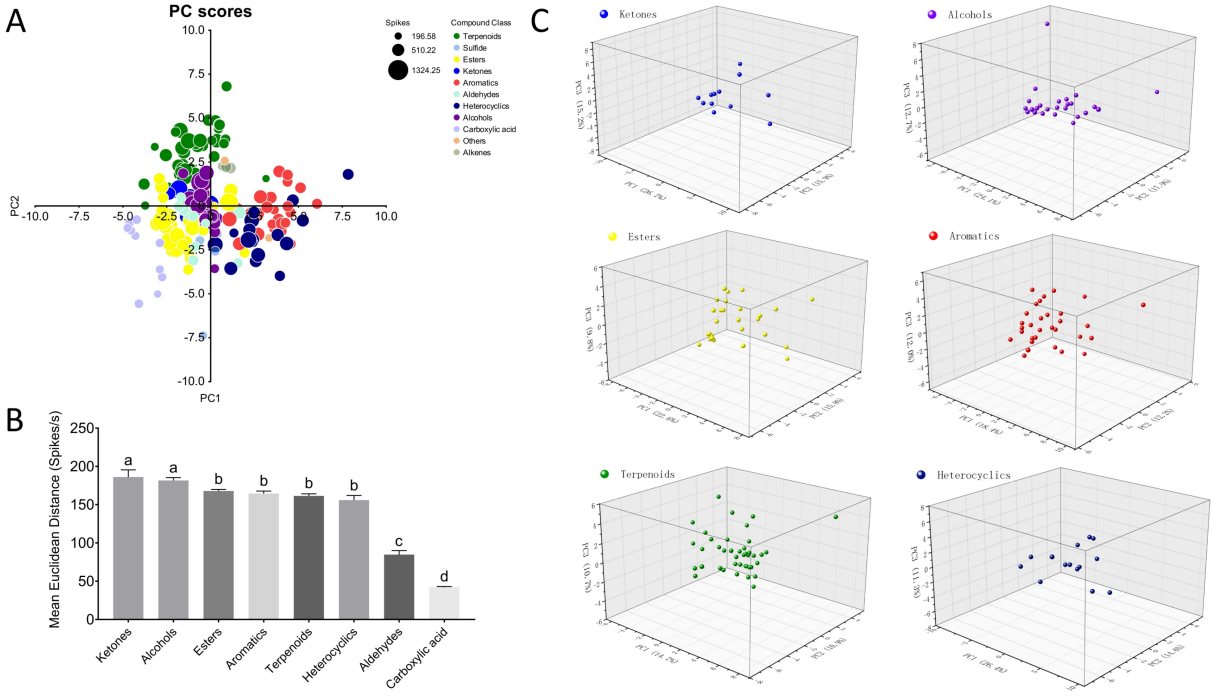
695 Figure 3. Correlations of the spatial antennal distribution of *Ae. albopictus* ORs with their
696 phylogeny and chromosomal locations. (A) Correlation between the antennal spatial distribution
697 of *AalbORs* and their phylogenetic relationships. The phylogenetic tree of AalbORs was
698 constructed using the maximum likelihood method. Bootstrap values were obtained from 1,000
699 maximum likelihood replicates; support rates were shown at each node by circles, with the
700 scale indicating values from 0 to 1. (B) Chromosomal locations of *AalbORs* and their
701 corresponding spatial distribution patterns in the antenna. The map employs a vertical
702 chromosomal coordinate axis (range: 0–600 Mb) to illustrate the genomic positions of *AalbORs*.
703 Red-marked *AalbORs* denote distally distributed *ORs*, blue-marked *AalbORs* mainly expressed
704 in the proximal domain, and green-marked *AalbORs* indicate *ORs* with uniform expression
705 across the entire antenna.

Langtaosha (LTS) Preprint doi: https://doi.org/10.65215/LTSpreprints.2026.10.20.000364. This version posted October 20, 2026. The copyright holder for this preprint (which was not certified by peer review) is the author/funder. Creative Commons license: CC Attribution-NonCommercial-NoDerivatives 4.0 https://creativecommons.org/licenses/by-nc-nd/4.0



706

707 Figure 4. Response profiles of AalbORs to a broad panel of compounds. (A) Representative
708 response traces of ab3 sensillum in the control fly line (*OR22ab*$^{-/-}$*Gal4*) and the AalbOR-
709 expressing fly line (*OR22ab*$^{-/-}$*Gal4; UAS-AalbOR*) elicited by selected chemical compounds. (B)
710 Heatmap showing responses of 33 heterologously expressed AalbORs to the chemical panel.
711 Odorants were diluted to 1% (w/v for solid, v/v for liquid) in paraffin oil or DMSO (n=3–5).

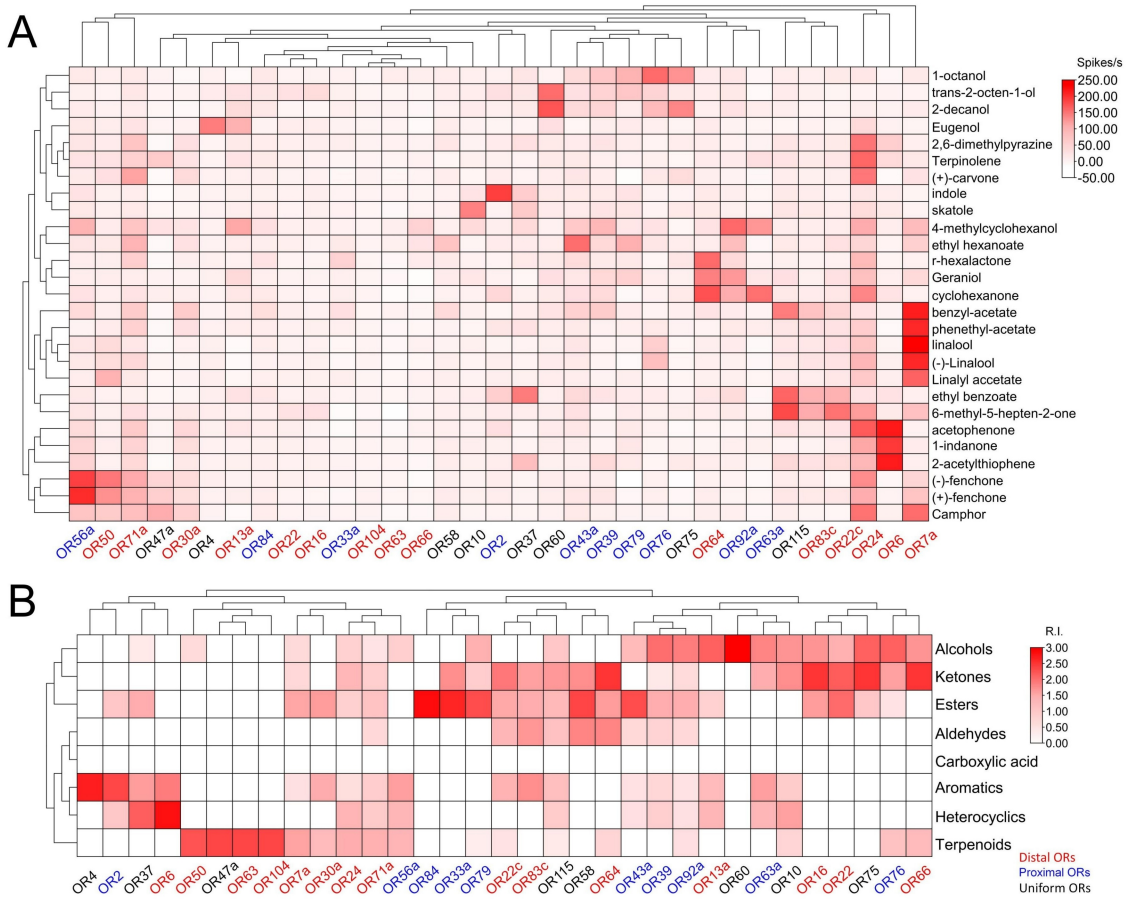


712

713 Figure 5. Odorant space of AalbORs and the relative discriminative ability of AalbORs towards
714 major chemical classes. (A) Two-dimensional PCA projection of odor space represented by
715 AalbORs. (B) Mean Euclidean distances of major chemical classes discriminated by AalbORs.

Langtaosha (LTS) Preprint doi: https://doi.org/10.65215/LTSpreprints.2026.10.20.000364. This version posted October 20, 2026. The copyright holder for this preprint (which was not certified by peer review) is the author/funder. Creative Commons license: CC Attribution-NonCommercial-NoDerivatives 4.0 https://creativecommons.org/licenses/by-nc-nd/4.0

716 Error bars represent the standard error of the mean (SEM). Statistical significance among
717 chemical classes was determined using one-way ANOVA; letters above bars denote significant
718 differences ($p<0.05$). Groups sharing the same letter are not statistically distinct. (C) Three-
719 dimensional PCA visualization of intra-class odorant dispersion.

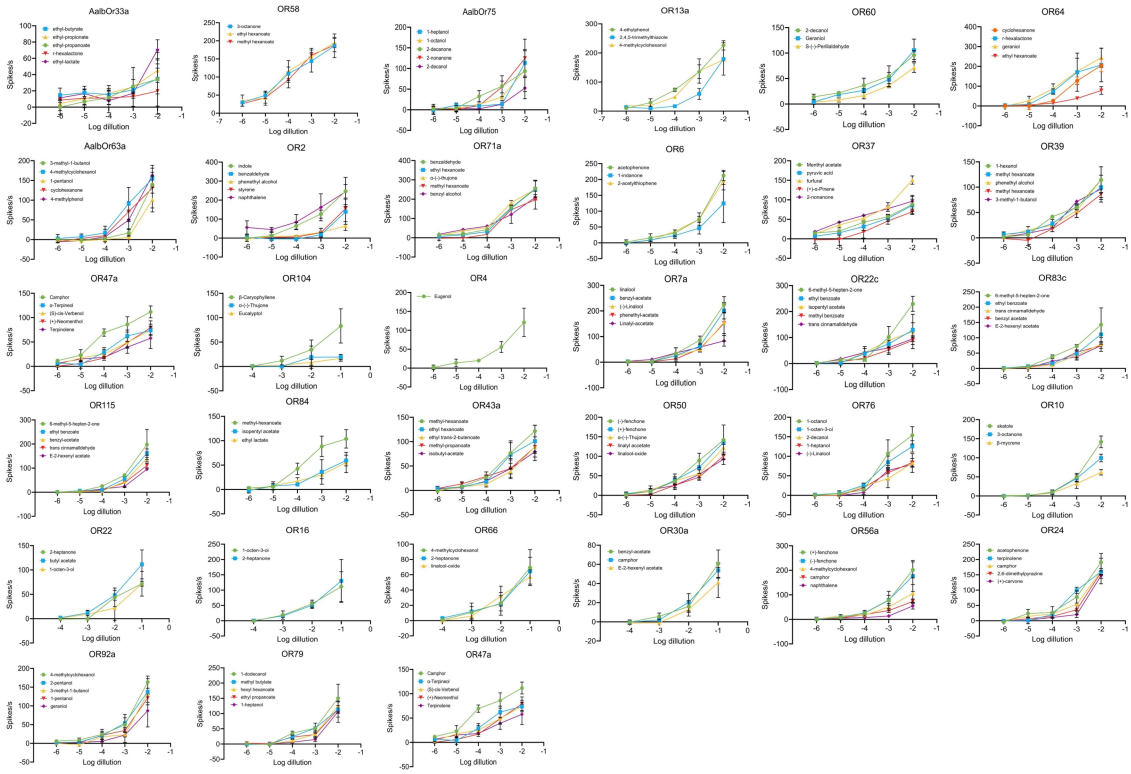


720

721 Figure 6. Correlation analysis of differentially distributed AalbORs and their functional specificity
722 to individual compounds or compound groups. (A) The coding map of AalbORs against
723 compounds that elicited extremely strong responses (≥150 spikes/s) in at least one AalbOR.
724 (B) Heatmap showing the response preference (Response Index, RI) of AalbORs to major
725 chemical groups. Response Index (RI) was calculated by dividing the ratio of one OR's active
726 excitatory response induced by a specific chemical category by the proportion of that chemical
727 category in the test panel. Bottom annotations of AalbORs denote spatial distribution patterns:
728 distal (marked in red), proximal (marked in blue), and uniform (marked in gray).

Langtaosha (LTS) Preprint doi: https://doi.org/10.65215/LTSpreprints.2026.10.20.000364. This version posted October 20, 2026. The copyright holder for this preprint (which was not certified by peer review) is the author/funder. Creative Commons license: CC Attribution-NonCommercial-NoDerivatives 4.0 https://creativecommons.org/licenses/by-nc-nd/4.0

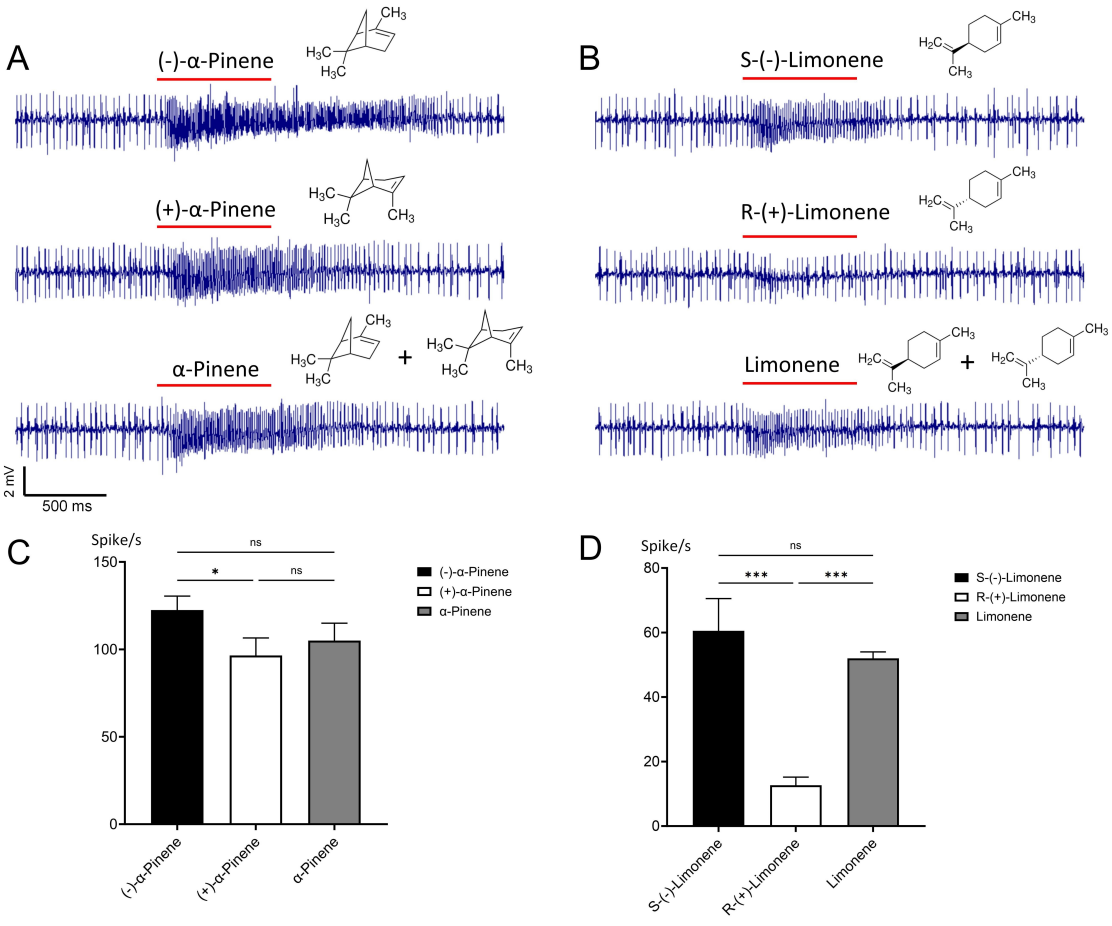
729



730

731 Figure S1. Dose-dependent responses of AalbORs to different compounds. Dose-response
732 curves were generated for various AalbORs in response to their respective odorant ligands.
733 The X-axis represents the log dilution of odorants, and the Y-axis represents the neuronal
734 response (spikes/s). Data are presented as mean ± SEM (n = 3–5).

Langtaosha (LTS) Preprint doi: https://doi.org/10.65215/LTSpreprints.2026.10.20.000364. This version posted October 20, 2026. The copyright holder for this preprint (which was not certified by peer review) is the author/funder. Creative Commons license: CC Attribution-NonCommercial-NoDerivatives 4.0 https://creativecommons.org/licenses/by-nc-nd/4.0



735

736 Figure S2. AalbOR24 discriminated stereochemical differences in chiral enantiomers. (A)
737 Excitatory responses of AalbOR24 to (−)-α-Pinene and (+)-α-Pinene. (B) Excitatory
738 responses of AalbOR24 to R-(+)-Limonene and S-(−)-Limonene. (C) Significantly stronger
739 response of AalbOR24 to (−)-α-Pinene than to (+)-α-Pinene. (D) Significantly stronger
740 response of AalbOR24 to S-(−)-Limonene than to R-(+)-Limonene. Statistical significance was
741 determined by one-way ANOVA; *P < 0.05, ***P < 0.001; ns (not significant), P ≥ 0.05.

Langtaosha (LTS) Preprint doi: https://doi.org/10.65215/LTSpreprints.2026.10.20.000364. This version posted October 20, 2026. The copyright holder for this preprint (which was not certified by peer review) is the author/funder. Creative Commons license: CC Attribution-NonCommercial-NoDerivatives 4.0 https://creativecommons.org/licenses/by-nc-nd/4.0

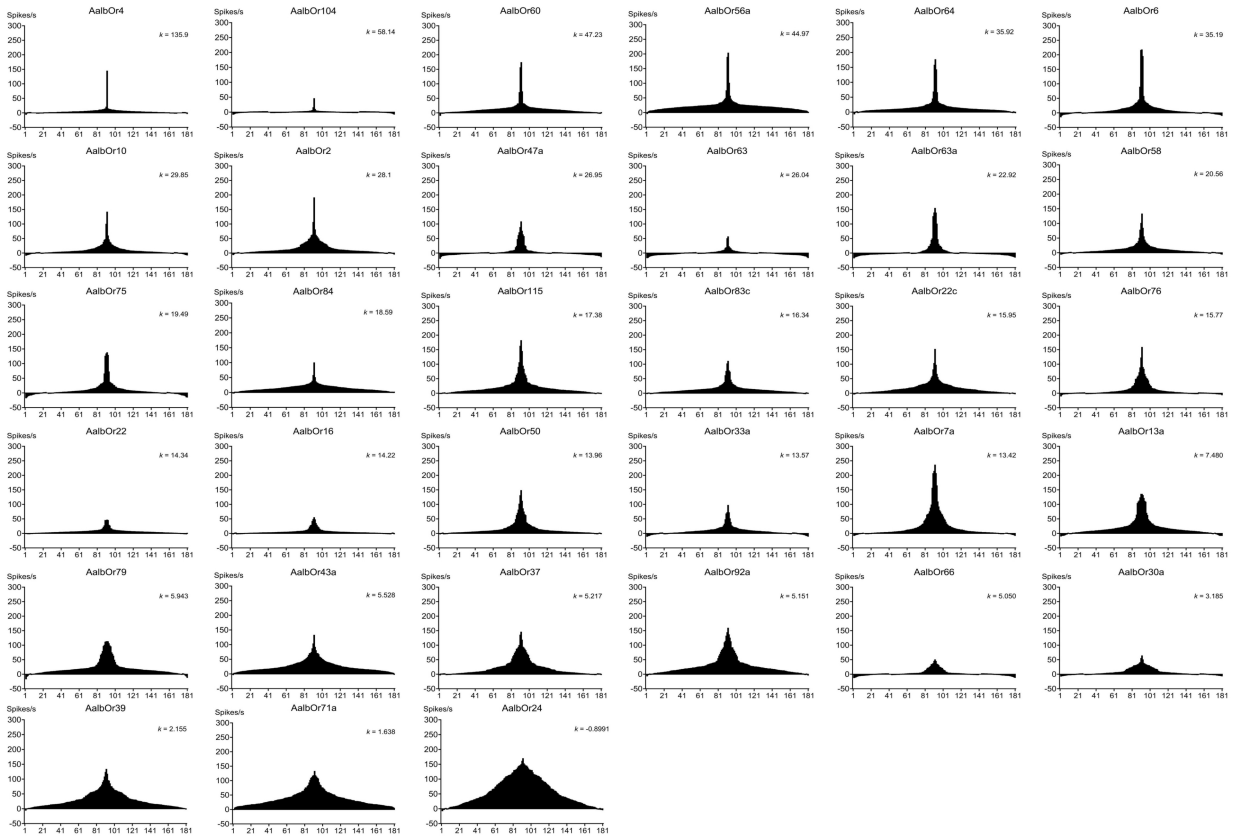
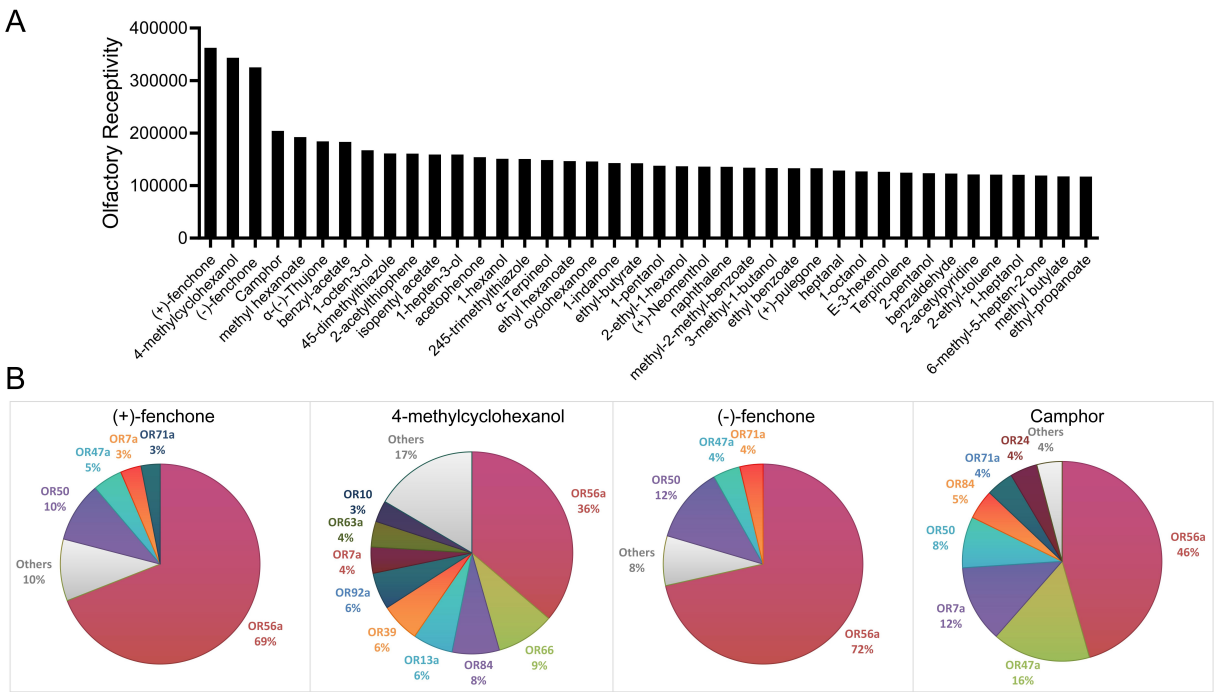


Figure S3. Tuning curves of individual AalbORs. Tuning curves for the AalbORs that respond to at least one odorant on the panel (≥ 50 spikes/s). The x-axis represents a panel of 180 odorants with the most potent ligand for each receptor placed at the center. The breadth of each tuning curve was quantified using the kurtosis value (K value), which depicts the "peakedness" of the response distribution.

Langtaosha (LTS) Preprint doi: https://doi.org/10.65215/LTSpreprints.2026.10.20.000364. This version posted October 20, 2026. The copyright holder for this preprint (which was not certified by peer review) is the author/funder. Creative Commons license: CC Attribution-NonCommercial-NoDerivatives 4.0 https://creativecommons.org/licenses/by-nc-nd/4.0



748

749 Figure S4. Conceptualized receptivity of *Ae. albopictus* to various compounds. (A) Calculated
750 olfactory receptivity of *Ae. albopictus* to the tested panel of compounds in this study, with the
751 top 40 most robust compounds displayed. The olfactory receptivity to each compound was
752 calculated as the sum of the SSR response for each OR multiplied by its relative
753 transcriptomic abundance. (B) Detailed contributions (>3%) of each AalbOR in perceiving the
754 most receptive compounds were presented, with AalbOR56a consistently showing the largest
755 contributions across these four odors.

Langtaosha (LTS) Preprint doi: https://doi.org/10.65215/LTSpreprints.2026.10.20.000364. This version posted October 20, 2026. The copyright holder for this preprint (which was not certified by peer review) is the author/funder. Creative Commons license: CC Attribution-NonCommercial-NoDerivatives 4.0 https://creativecommons.org/licenses/by-nc-nd/4.0

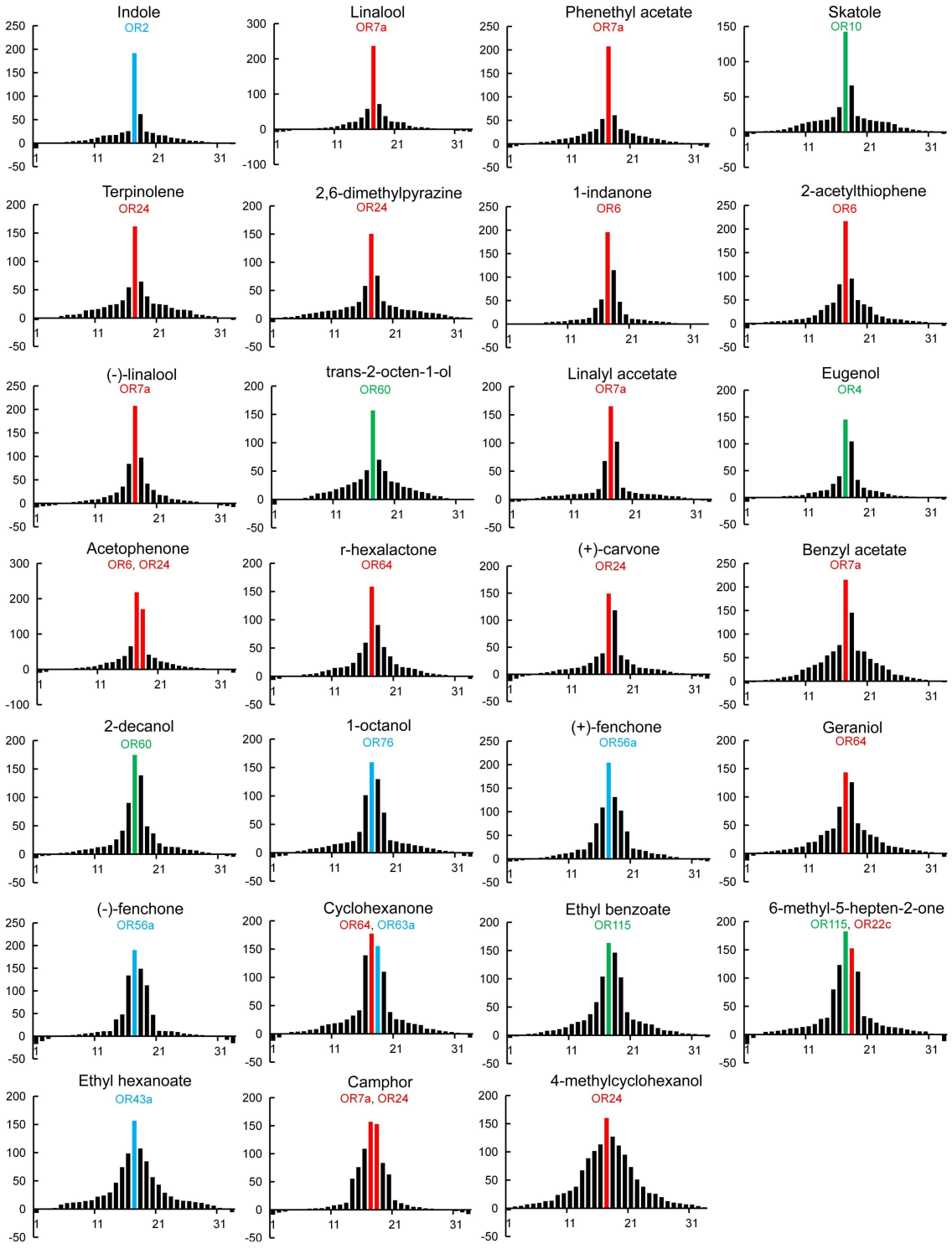


Figure S5. Odorant tuning curves. Tuning curves are shown for odorants eliciting strong excitatory responses (≥150 spikes/s) in at least one AalbOR. The x-axis represents different odorant receptors, with the receptor exhibiting the strongest response to each odorant positioned centrally. Odorant responses are color-coded according to receptor expression patterns: blue markers denote proximally expressed AalbORs, red markers denote distally expressed AalbORs, and green markers denote uniformly expressed AalbORs.

Langtaosha (LTS) Preprint doi: https://doi.org/10.65215/LTSpreprints.2026.10.20.000364. This version posted October 20, 2026. The copyright holder for this preprint (which was not certified by peer review) is the author/funder. Creative Commons license: CC Attribution-NonCommercial-NoDerivatives 4.0 https://creativecommons.org/licenses/by-nc-nd/4.0

763 Supplementary Table 1. Primers used for generating the *AalbORs-QF2* driver lines

764

AalbORs	gene ID	forward primer	reverse primer
pAalbOR99	LOC109408879	TATACGAAGTTATACGCGTCGAAGTC CGGGATTCGGGTGTTGGTCGTGTT	GCTTGGGTGGCATCCTAGGCTCGAGGTTTG ACACAATCCACCGTTCTGATGTACG
pAalbOR43a	LOC115266245	TATACGAAGTTATACGCGTCACAACAT CAATTTTTCCCTGAAGAAGACGC	GCTTGGGTGGCATCCTAGGCTCGAGTATGA TTCCTTTTTAAATACCGGAGTACAG
PAalbOR41	LOC109418739	TATACGAAGTTATACGCGTCTATACAC ACTGGGAATAATGTTATTAATAT	GCTTGGGTGGCATCCTAGGCTCGAGCTTGA CTGGTTCCGGTAGATTGCGTACTTT

765

766 Supplementary Table 2. Primers for the construction of *Drosophila* empty neuron strains
767 expressing AalbORs.

AalbORs	gene ID	forward primer	reverse primer
OR4	LOC109400239	GGGAATTGGGAATTCATGGGACAATTCG ACGACTTCAT	TCTGTTAACGAATTCCTACTTGTTCTTTTC TTGACTGT
OR7a	LOC109433291	GGGAATTGGGAATTCATGGAGCTCAAGA AAGTTAGACA	TCTGTTAACGAATTCTTAAGATTTTCGCATA GTGCGCA
OR22c	LOC109399842	gaattcATGGATTACCTAGCAAAGT	CTCGAGTTATTCAGTAAATTGCATC
OR83c	LOC109405928	GGGAATTGGGAATTCATGAGTTTTATTAA GAAACTACA	TCTGTTAACGAATTCTTATTCTTCGCGTAC AGTGAGAA
OR115	LOC134291832	GGGAATTGGGAATTCATGCGAAGTGACT TCACATCGAA	TCTGTTAACGAATTCTCAATCACTGGTTTG AAGCTTAC
OR63a	LOC109429627	gaattcATGTACAACACTCACCCGG	CTCGAGCTAAAACCTTTTCTTCAG
OR43a	LOC115266245	GGGAATTGGGAATTCATGGAACGATTCG AACGTTATTT	TCTGTTAACGAATTCCTAGTTGAAACTCTG CAGCATCG
OR50	LOC109430000	GGGAATTGGGAATTCATGCGGTCGGTCA TCAAACTTCT	TCTGTTAACGAATTCTCATTTGCACCTCGC TGAGATGC
OR76	LOC115259618	GGGAATTGGGAATTCATGTCCGCCCGTA CGGATTTCCT	TCTGTTAACGAATTCCTAGTCCTGAACCAT GTTCATCAAGAGCG
OR60	LOC109414782	GGGAATTGGGAATTCATGGCTAATCTTT GGCTCAACCA	TCTGTTAACGAATTCCTACTTTCTAAACGT CCAAAGGAACATTG
OR64	LOC109419312	GGAATTGGGAATTCATGGACGACCGCCT CATA	TGTTAACGAATTCTTATAAGTTTTGTAGCAT
OR37	LOC109401998	GGGAATTGGGAATTCATGGTTGACACGC AGCTCTCTCC	TCTGTTAACGAATTCTCAGGTCATTACACT GGATATACGGAAGGCAG
OR22	LOC109397072	GGGAATTGGGAATTCTTACTTGAAAGTG TT	TCTGTTAACGAATTCTCTGGTGATGGTTTA GTGCAGAA
OR16	LOC109404361	GGGAATTGGGAATTCTTCTCCAGGTACC ATGGATACAT	TCTGTTAACGAATTCATACAAATTTAAAATC ATGCGGT
OR66	LOC109419901	GGGAATTGGGAATTCCCTCGTTCGTACC AACAAAATTA	TCTGTTAACGAATTCTATTTTACTATAGGGA CTTTCAGCCC

Langtaosha (LTS) Preprint doi: https://doi.org/10.65215/LTSpreprints.2026.10.20.000364. This version posted October 20, 2026. The copyright holder for this preprint (which was not certified by peer review) is the author/funder. Creative Commons license: CC Attribution-NonCommercial-NoDerivatives 4.0 https://creativecommons.org/licenses/by-nc-nd/4.0

OR30a	LOC109418186	GGGAATTGGGAATTCATGACACCGCTAGAAGACTACTA	CCCTCTGTTAACGAATTCTTATTCAACATACTGCAAAATCA
OR13a	LOC109411170	GGGAATTGGGAATTCATGGAGCAGTACCTGCAGAAAAT	TCTGTTAACGAATTCTCATATACTGACCGCGATGAAGG
OR24	LOC109399953	GGGAATTGGGAATTCATGAGTTTCCTGAAGAAACTTCA	TCTGTTAACGAATTCTTACGTCAGATGTTCCTGATGTCGTTGGATGA
OR2	LOC109416825	gaattcATGTTGATCGAAAACTGC	CTCGAGTTAATTATAAACTCTCCG
OR92a	LOC109623406	GGGAATTGGGAATTCATGGAATCGATTATCAAGCTACT	TCTGTTAACGAATTCTCAACGTGAGTCCAGCATCTGTCGTAGGA
OR58	LOC109412278	GGGAATTGGGAATTCATGATTTTCATTATCAAGACCTA	TCTGTTAACGAATTCTTACTCCAACACACTGGTCAGCA
OR47a	LOC109623405	GGGAATTGGGAATTCATGGAATCGATTATCAAGCTGCT	TCTGTTAACGAATTCTCAACGTGACTCCAGCATCTGCC
OR63	LOC109419306	GGGAATTGGGAATTCATGTTCCTCAAGAAGACAGCTCA	TCTGTTAACGAATTCTTAGAAGCCATTTTTCAGTAACA
OR104	LOC109417564	GGGAATTGGGAATTCTTATTTAACGTCTATCGGAGGAT	TCTGTTAACGAATTCTGGCGAACATCTGGTCCGT
OR75	LOC134285539	GGGAATTGGGAATTCTGTTGTTATTGATTATGAAATT	TCTGTTAACGAATTCATTTTTCTTAGTCTCGAAATTAA
OR33a	LOC134286592	GGGAATTGGGAATTCCTATCGTTTCCTTTTTCATTCCG	TCTGTTAACGAATTCAGAATAGTTGCTTTTTTATTCAA

768

769 Supplementary Table 3. Compounds used in single sensillum recordings

770

Chemicals	Chemical class	CAS	Company	Purity
methanol	Alcohols	67-56-1	Macklin	99.80%
1-propanol	Alcohols	71-23-8	Macklin	99.50%
1-butanol	Alcohols	71-36-3	Macklin	99.50%
1-pentanol	Alcohols	71-41-0	Macklin	99.50%
2-pentanol	Alcohols	6032-29-7	Macklin	98%
1-hexanol	Alcohols	111-27-3	Macklin	99.50%
1-heptanol	Alcohols	111-70-6	Macklin	99.50%
1-octanol	Alcohols	111-87-5	Macklin	99.50%
1-dodecanol	Alcohols	112-53-8	Macklin	98%
3-methyl-1-butanol	Alcohols	123-51-3	Macklin	99%
3-methyl-2-buten-1-ol	Alcohols	556-82-1	Macklin	98%
2-ethyl-1-hexanol	Alcohols	104-76-7	Macklin	98%
1-penten-3-ol	Alcohols	616-25-1	Macklin	98%
1-hexen-3-ol	Alcohols	4798-44-1	Macklin	98%
1-hepten-3-ol	Alcohols	4938-52-7	Macklin	98%
1-octen-3-ol	Alcohols	3391-86-4	Macklin	98%
Z2-hexenol	Alcohols	928-94-9	Sigma	95%

Langtaosha (LTS) Preprint doi: https://doi.org/10.65215/LTSpreprints.2026.10.20.000364. This version posted October 20, 2026. The copyright holder for this preprint (which was not certified by peer review) is the author/funder. Creative Commons license: CC Attribution-NonCommercial-NoDerivatives 4.0 https://creativecommons.org/licenses/by-nc-nd/4.0

E-2-hexenol	Alcohols	928-95-0	Macklin	97%
trans-2-octen-1-ol	Alcohols	18409-17-1	Macklin	98%
2-decanol	Alcohols	1120-06-5	Macklin	98%
E-3-hexenol	Alcohols	928-97-2	Macklin	97%
4-methylcyclohexanol	Alcohols	589-91-3	Macklin	98%
2,3-butanediol	Alcohols	513-85-9	Macklin	98%
furfural	Aldehydes	98-01-1	Macklin	98%
trans cinnamalldehyde	Aldehydes	14371-10-9	Macklin	98%
propional	Aldehydes	123-38-6	Macklin	97%
butanal	Aldehydes	123-72-8	Macklin	98%
isobutanal	Aldehydes	78-84-2	Macklin	98%
2-methylbutanal	Aldehydes	96-17-3	Macklin	98%
pentanal	Aldehydes	110-62-3	Macklin	98%
hexanal	Aldehydes	66-25-1	Macklin	98%
heptanal	Aldehydes	111-71-7	Macklin	95%
octanal	Aldehydes	124-13-0	Macklin	95%
nonanal	Aldehydes	124-19-6	Macklin	98%
decanal	Aldehydes	112-31-2	Macklin	95%
acetaldehyde	Aldehydes	75-07-0	Macklin	99.50%
trans-2-octene	Alkenes	13389-42-9	Macklin	98%
trans-3-octene	Alkenes	14919-01-8	Macklin	98%
trans-4-octene	Alkenes	14850-23-8	Macklin	98%
phenol	Aromatics	108-95-2	Macklin	99.60%
benzaldehyde	Aromatics	100-52-7	Macklin	98.50%
benzyl alcohol	Aromatics	100-51-6	Macklin	99%
benzyl acetate	Aromatics	140-11-4	Macklin	99%
acetophenone	Aromatics	98-86-2	Macklin	98%
benzyl methyl ether	Aromatics	538-86-3	Macklin	98%
estragole	Aromatics	140-67-0	Macklin	98%
2-methylphenol	Aromatics	95-48-7	Macklin	98%
3-methylphenol	Aromatics	108-39-4	Macklin	98%
4-methylphenol	Aromatics	106-44-5	Macklin	98%
2-ethylphenol	Aromatics	90-00-6	Macklin	98%
4-ethylphenol	Aromatics	123-07-9	Macklin	98%
2-propylphenol	Aromatics	644-35-9	Macklin	98%
methyl benzoate	Aromatics	93-58-3	Macklin	98%
methyl-2-methyl-benzoate	Aromatics	89-71-4	Macklin	98%
ethyl benzoate	Aromatics	93-89-0	Macklin	98%
dimethyl phthalate	Aromatics	131-11-3	Macklin	98%
phenylacetaldehyde	Aromatics	122-78-1	Macklin	95%
phenethyl acetate	Aromatics	103-45-7	Macklin	99%
phenethyl alcohol	Aromatics	60-12-8	Macklin	98%
2-ethyl-toluene	Aromatics	611-14-3	Macklin	98%
benzene	Aromatics	71-43-2	Macklin	99%

Langtaosha (LTS) Preprint doi: https://doi.org/10.65215/LTSpreprints.2026.10.20.000364. This version posted October 20, 2026. The copyright holder for this preprint (which was not certified by peer review) is the author/funder. Creative Commons license: CC Attribution-NonCommercial-NoDerivatives 4.0 https://creativecommons.org/licenses/by-nc-nd/4.0

ethyl benzene	Aromatics	100-41-4	Macklin	99%
propylbenzene	Aromatics	103-65-1	Macklin	98%
styrene	Aromatics	100-42-5	Macklin	99%
xylene	Aromatics	1330-20-7	Macklin	98%
decanoic acid	Carboxylic acid	334-48-5	Macklin	98%
undecanoic acid	Carboxylic acid	112-37-8	Macklin	98%
dodecanoic acid	Carboxylic acid	143-07-7	Macklin	98%
tridecanoic acid	Carboxylic acid	638-53-9	Macklin	98%
linoleic acid	Carboxylic acid	60-33-3	Macklin	99%
butanoic-acid	Carboxylic acid	107-92-6	Macklin	98%
hexanoic-acid	Carboxylic acid	21188-58-9	Macklin	98%
L(+)-lactic-acid	Carboxylic acid	79-33-4	Macklin	98%
pyruvic acid	Carboxylic acid	127-17-3	Macklin	98%
N-Valeric acid	Carboxylic acid	109-52-4	Macklin	99%
r-hexalactone	lactone	695-06-7	Macklin	99%
r-octalactone	lactone	104-50-7	Macklin	99.00%
ethyl cinnamate	Ester	103-36-6	Macklin	98%
methyl-salicylate	Ester	119-36-8	Macklin	98%
ethyl-formate	Ester	109-94-4	Macklin	99%
ethyl-acetate	Ester	141-78-6	Macklin	99.80%
propyl-acetate	Ester	109-60-4	Macklin	99%
methyl acetate	Ester	79-20-9	Macklin	99.50%
butyl acetate	Ester	123-86-4	Macklin	99%
isobutyl-acetate	Ester	110-19-0	Macklin	99%
isopentyl acetate	Ester	123-92-2	Macklin	99%
pentyl acetate	Ester	628-63-7	Macklin	99%
E-2-hexenyl acetate	Ester	2497-18-9	Macklin	99.80%
hexyl acetate	Ester	142-92-7	Macklin	98%
ethyl-propanoate	Ester	105-37-3	Macklin	99%
methyl butylate	Ester	623-42-7	Macklin	98%
methyl-propanoate	Ester	554-12-1	Macklin	98%
ethyl-butyrate	Ester	105-54-4	Macklin	98%
hexyl butyrate	Ester	2639-63-6	Macklin	98%
ethyl-hexanoate	Ester	123-66-0	Macklin	99%
ethyl-3-hydroxybutyrate	Ester	5405-41-4	Macklin	98%
methyl hexanoate	Ester	106-70-7	Macklin	98%
hexyl hexanoate	Ester	6378-65-0	Macklin	98%
methyl-octanoate	Ester	111-11-5	Macklin	98%
ethyl octanoate	Ester	106-32-1	Macklin	98%
methyl nanonate	Ester	1731-84-6	Macklin	98%
ethyl trans-2-butenoate	Ester	623-70-1	Macklin	98%
ethyl-lactate	Ester	97-64-3	Macklin	98%
naphthalene	Heterocyclics	91-20-3	Macklin	98%
cinnamyl alcohol	Heterocyclics	104-54-1	Macklin	98%

Langtaosha (LTS) Preprint doi: https://doi.org/10.65215/LTSpreprints.2026.10.20.000364. This version posted October 20, 2026. The copyright holder for this preprint (which was not certified by peer review) is the author/funder. Creative Commons license: CC Attribution-NonCommercial-NoDerivatives 4.0 https://creativecommons.org/licenses/by-nc-nd/4.0

coumarin	Heterocyclics	91-64-5	Macklin	98%
indole	Heterocyclics	120-72-9	Macklin	98%
skatole	Heterocyclics	83-34-1	Macklin	98%
2-picoline	Heterocyclics	109-06-8	Macklin	98%
2-methylfunan	Heterocyclics	534-22-5	Macklin	98%
2,6-dimethylpyrazine	Heterocyclics	108-50-9	Macklin	98%
2-acetylthiophene	Heterocyclics	88-15-3	Macklin	98%
thiazole	Heterocyclics	288-47-1	Macklin	98%
4-methylthiazole	Heterocyclics	693-95-8	Macklin	98%
2-acetylthiazole	Heterocyclics	24295-03-2	Macklin	98%
2-ethoxythiazole	Heterocyclics	15679-19-3	Macklin	98%
2-iso-butyl-thiazole	Heterocyclics	18640-74-9	Macklin	98%
4,5-dimethylthiazole	Heterocyclics	3581-91-7	Macklin	98%
2,4,5-trimethylthiazole	Heterocyclics	13623-11-5	Macklin	98%
2-acetylpyridine	Heterocyclics	1122-62-9	Macklin	98%
2-heptanone	Ketones	110-43-0	Macklin	99%
3-octanone	Ketones	106-68-3	Macklin	98%
2-nonanone	Ketones	821-55-6	Macklin	99%
6-methyl-5-hepten-2-one	Ketones	110-93-0	Macklin	98%
2,3-butanedione	Ketones	431-03-8	Macklin	98%
cyclohexanone	Ketones	108-94-1	Macklin	99%
2-pentanone	Ketones	107-87-9	Macklin	98%
3-pentanone	Ketones	96-22-0	Macklin	98%
2-hexanone	Ketones	591-78-6	Macklin	99%
2-decanone	Ketones	693-54-9	Macklin	99.50%
1-indanone	Ketones	83-33-0	Macklin	98%
DEET	Others	134-62-3	Macklin	98%
ammonia	Others	7664-41-7	Macklin	99.50%
3-methylthio-1-propanol	Sulfide	505-10-2	Macklin	98%
dimethylsulfide	Sulfide	75-18-3	Macklin	99%
carbon disulfide	Sulfide	75-15-0	Macklin	99.50%
methyl disulfide	Sulfide	624-92-0	Macklin	98%
Terpinolene	Terpenoids	586-62-9	Sigma	95%
α-Terpinene	Terpenoids	99-86-5	Macklin	95%
β-mycrene	Terpenoids	123-35-3	Sigma	90.00%
S-(−)-Limonene	Terpenoids	5989-54-8	Macklin	95%
R-(+)-Limonene	Terpenoids	5989-27-5	Macklin	99%
limonene	Terpenoids	138-86-3	Macklin	95%
1S-(+)-3-Carene	Terpenoids	498-15-7	Macklin	90%
3-carene	Terpenoids	13466-78-9	Macklin	90%
α-Pinene	Terpenoids	80-56-8	Macklin	98%
(−)-α-Pinene	Terpenoids	7785-26-4	Macklin	98%
(+)-α-Pinene	Terpenoids	7785-70-8	Macklin	98%
(−)-β-Pinene	Terpenoids	18172-67-3	Macklin	95%

Langtaosha (LTS) Preprint doi: https://doi.org/10.65215/LTSpreprints.2026.10.20.000364. This version posted October 20, 2026. The copyright holder for this preprint (which was not certified by peer review) is the author/funder. Creative Commons license: CC Attribution-NonCommercial-NoDerivatives 4.0 https://creativecommons.org/licenses/by-nc-nd/4.0

Thymol	Terpenoids	89-83-8	Macklin	99.00%
Menthol	Terpenoids	2216-51-5	Macklin	99.50%
Citronellol	Terpenoids	106-22-9	Macklin	95%
Geranyl acetate	Terpenoids	105-87-3	Macklin	96%
(−)-carvone	Terpenoids	6485-40-1	Macklin	99%
(+)-carvone	Terpenoids	2244-16-8	Macklin	99%
(−)-fenchone	Terpenoids	7787-20-4	Macklin	98%
(+)-fenchone	Terpenoids	4695-62-9	Macklin	97%
citronellal	Terpenoids	106-23-0	Macklin	96%
linalool-oxide	Terpenoids	60047-17-8	Macklin	97%
Citronellic acid	Terpenoids	57030-77-0	Macklin	97%
Geranyl acetone	Terpenoids	3796-70-1	Macklin	95%
(+)-Terpinen-4-ol	Terpenoids	2438-10-0	Macklin	98%
nerol	Terpenoids	106-25-2	Macklin	98%
linalool	Terpenoids	78-70-6	Macklin	98%
(−)-Linalool	Terpenoids	126-91-0	Macklin	97%
(S)-cis-Verbenol	Terpenoids	18881-04-4	Macklin	95%
Menthyl acetate	Terpenoids	89-48-5	Macklin	98%
S-(−)-Perillaldehyde	Terpenoids	18031-40-8	Macklin	90%
α-Terpineol	Terpenoids	98-55-5	Macklin	98%
Linalyl accetate	Terpenoids	115-95-7	Macklin	98%
(−)-Menthone	Terpenoids	14073-97-3	Macklin	98%
Geraniol	Terpenoids	106-24-1	Macklin	98%
citral	Terpenoids	5392-40-5	Macklin	97%
Camphor	Terpenoids	76-22-2	Macklin	96%
Eucalyptol	Terpenoids	470-82-6	Macklin	99.50%
β-Caryophyllene	Terpenoids	87-44-5	Sigma	97%
α-(−)-Thujone	Terpenoids	546-80-5	Macklin	98%
(+)-pulegone	Terpenoids	89-82-7	Macklin	98%
(+)-Neomenthol	Terpenoids	2216-52-6	Macklin	98%
Eugenol	Terpenoids	97-53-0	Macklin	99%

771